ACS Sustainable Chemistry & Engineering

pubs.acs.org/journal/ascecg

Perspective

Chitosan-Based N-Doped Carbon Materials for Electrocatalytic and Photocatalytic Applications

Ayesha Khan,* Michael Goepel, Juan Carlos Colmenares,* and Roger Gläser*

Cite This: *ACS Sustainable Chem. Eng.* 2020, 8, 4708−4727

Read Online

ACCESS | Metrics & More | Article Recommendations

ABSTRACT: Chitosan-derived N-doped carbon materials are attractive candidates for the preparation of catalysts with a wide range of applications. Chitosan is a nitrogen rich (∼7 wt %) renewable biomass resource derived from seafood waste. Nitrogen-containing functional groups (amine and acetamide) of chitosan make it a suitable precursor for the synthesis of N-doped carbon materials. This perspective provides an overview on various techniques for the preparation and characterization of chitosan-based N-doped carbon materials and their application in the field of electrocatalysis and photocatalysis. Additional doping with nitrogen imparts greater electrochemical stability and basic character to the material due to the ability of nitrogen atoms to accept electrons. Nevertheless, each type of C−N bonding configuration has unique potential for catalytic reactions attributed to different electronic structure and catalytically active sites. The ability to acquire desired N-bonding states during the process of doping will provide a better control over the material application. The promising performance of chitosan-based N-doped carbon materials in electrocatalytic and photocatalytic reactions is attributed to their improved electronic structure and charge transfer properties. Moreover, research trends toward the design of chitosan-based N-doped carbons materials with required features for electrocatalytic and photocatalytic applications have also been identified.

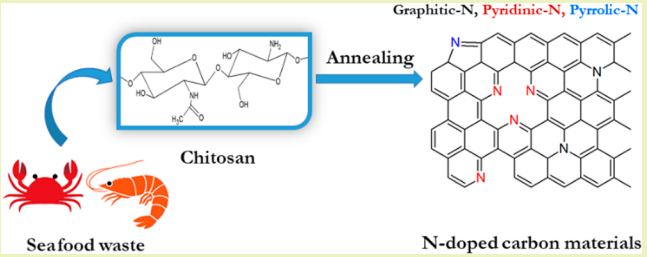

KEYWORDS: *Chitosan, N-doping, Electrocatalysis, Photocatalysis, Carbonization, Oxygen reduction reaction, Hydrogen generation, N-doped carbon*

INTRODUCTION

The recent decline in renewable fossil fuel resources and growing environmental problems led to a paradigm shift in the utilization of resources. Biomass valorization has recently gained considerable attention in an attempt to produce value-added fine chemicals as well as carbon-based functional materials. There has been growing interest in the use of polymer materials derived from biomass such as cellulose, lignin, and chitin for the preparation of carbon-supported catalysts due to their significant advantages of being nontoxic, biodegradable, and biocompatible.[1,2] Chitin is a straight chain biopolymer that is the second most abundant on Earth after cellulose. It is the building block of the exoskeleton of marine animals, like crabs, shrimps, and lobsters.[3] Annually, approximately 6−8 million tons of chitin waste (crab, shrimp, and lobster shells) are produced around the globe.[4] Nevertheless, the potential worth of the chitin waste for the chemical and material industries is largely overlooked. Unlike other biomass resources like cellulose and lignin, chitin is a nitrogen-rich polymer that offers a greater potential for the production of nitrogen-containing chemicals and materials. Chitin is a relatively underutilized resource due to its inherent insolubility in common (organic) solvents and the expensive and wasteful methods employed for the extraction of chemicals from it. These have restrained its application in various fields and make its valorization rather challenging. However, some industry branches have explored the potential of chitin and its derivative chitosan in the fields of biomedicine, food technology, and textiles.[5]

Chitosan, being derived from partial deacetylation of chitin, is also a biobased nitrogenous copolymer, made up of repeating units of N-acetyl-D-glucosamine and D-glucosamine (Figure 1).[3] Numerous methods are employed for the deacetylation of chitin such as steam explosion, alkali treatment, and enzymatic deacetylation, depending on the required degree of deacetylation in chitosan.[6] Highly concentrated (40%−60%) alkali treatment is the most widely used method for the deacetylation of chitin.[7] Moreover, the deacetylation of chitin is carried out to different extents depending upon the application of chitosan. Accordingly, chitosan with various degrees of deacetylation

Received: December 16, 2019
Revised: February 28, 2020
Published: March 8, 2020

https://dx.doi.org/10.1021/acssuschemeng.9b07522
ACS Sustainable Chem. Eng. 2020, 8, 4708−4727

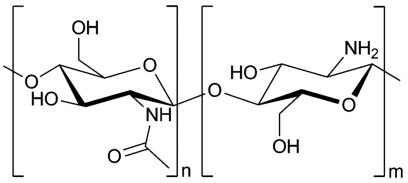

Figure 1. Chitosan, a linear polysaccharide composed of (1−4)-linked D-glucosamine and N-acetyl-D-glucosamine. Reprinted with permission from ref 10. Copyright (2014) Royal Society of Chemistry.

(DD) is formed. The molecular weight and DD are mainly responsible for determining the physicochemical properties of chitosan, specifically solubility. It has been reported that solubility of chitosan is directly related to DD and inversely related to the molecular weight.[8] Generally, it is soluble in acidic media and insoluble in basic and neutral media (such as water).[9]

On the other hand, chitosan has a high nitrogen content (~7 wt %)[11] due to the presence of nitrogen-containing functional groups (amine and acetamide) in its structure. This makes it a suitable precursor for the synthesis of N-doped carbon materials. These structural functional groups of chitosan are responsible for the nontoxic, biocompatible, and biodegradable properties of chitosan.[12] Moreover, it offers immense possibilities of chemical and mechanical modifications for the synthesis of novel N-doped carbon materials that have numerous advantages over its synthetic counterparts in terms of environmental and biomedical applications.[13] To date, various types of N-doped carbon materials have been prepared from chitosan, such as N-doped graphene quantum dots, graphene-like N-doped carbon nanosheets,[14] N-doped graphene aerogels,[15] and N-doped graphitic carbon nanoparticles.[16] The detailed descriptions of the synthesis procedure and application of these materials are discussed in the following sections. Nevertheless, the low reactivity and insolubility of chitosan in organic solvents are a few of the limitations associated with its application for the synthesis of N-doped carbon materials.[17]

This Perspective focuses on the preparation of chitosan-based N-doped carbon materials especially for electrocatalytic and photocatalytic applications to demonstrate the potential of chitosan in these emerging fields. Although, there have been some studies carried out in the past (over a decade ago) on the applications of chitosan (as catalyst and catalyst support) in heterogeneous catalysis (thermal catalysis) and enzymatic catalysis for the synthesis of fine chemicals and biochemical applications, respectively,[18,19] these domains will not be covered here. Instead of covering the whole range of applications in heterogeneous catalysis, the focus is on the potential of chitosan-based N-doped carbon materials for electrocatalysis and photocatalysis.

N-DOPED CARBON MATERIALS AND C−N BONDING CONFIGURATIONS

Several efforts have been made to tailor the chemical and morphological properties of carbon-based materials for improved catalytic performance. Heteroatom (e.g., nitrogen, phosphorus, sulfur, and boron) introduction into carbon-based materials has shown remarkable improvements in various fields such as catalysis, supercapacitors, lithium ion batteries, and water splitting reactions.[20] For example, N-doping in graphitic carbon nitride (g-C_3N_4) improved the photocatalytic activity of the material for H_2 generation under visible light. The average H_2 generation rate upon doping increased from 15 to 64 μmol h^{-1}. This enhancement in the activity of the N-doped material ascribed to the improve light-harvesting properties, retardation in charge recombination and extended and delocalized π-conjugated system.[21]

Carbon-based materials are generally rich in oxygen-containing functional groups on the surface. This results in a p-doping effect due to the greater electronegativity of oxygen atoms compared to carbon atoms. Substituting oxygen functional groups on the surface with nitrogen-containing functional moieties can transform carbon-based nanomaterials into n-type semiconductors. These materials show both p- and n-type conductivities due to oxygen functionalities and nitrogen functionalities. The sp^2 clusters of carbon nanomaterials serve as the connection between the p- and n-domains to form a p−n junction that is responsible for the charge transfer at the interface.[22,23]

For the sake of this Perspective, N-doped carbon materials are considered materials where the incorporation of nitrogen atoms into carbonaceous materials occurs either into the aromatic carbon structure or as functional moieties attached to the carbon atom via covalent bonding. Commonly, three main bonding configurations have been identified in carbon materials when doped with nitrogen atoms (Figure 2), i.e., pyridinic-N, pyrrolic-

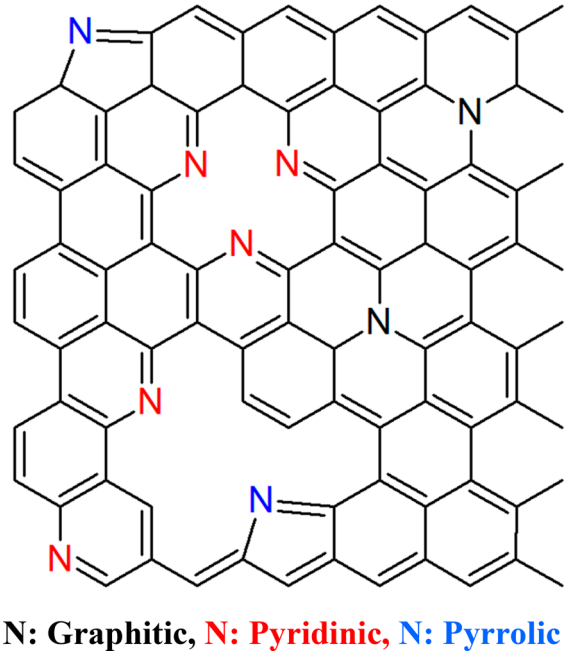

Figure 2. Three main bonding configurations (graphitic, pyridinic, and pyrrolic) in N-doped carbon materials. Reprinted with permission from ref 24. Copyright (2018) Elsevier.

N, and graphitic-N (quaternary-N).[24] Pyridinic-N atoms are bonded to two carbon atoms with a sp^2 configuration in a hexagonal structure and offer one p electron to the Π system. Pyrrolic-N is bonded with two other carbon atoms but with a sp^3 configuration and contributes two p electrons to the Π system, like in pyrrole, whereas a graphitic-N atom arises from the direct substitution of a carbon atom with a nitrogen atom, where the nitrogen atom is directly bonded to three carbon atoms with a sp^2 configuration. Besides the three common N types, aminic-N and pyridinic-N-oxides also been observed in N-doped carbon materials (N-graphene and N-carbon nanotubes).[25] Nevertheless, each type of C−N bonding configuration has a unique

https://dx.doi.org/10.1021/acssuschemeng.9b07522
ACS Sustainable Chem. Eng. 2020, 8, 4708−4727

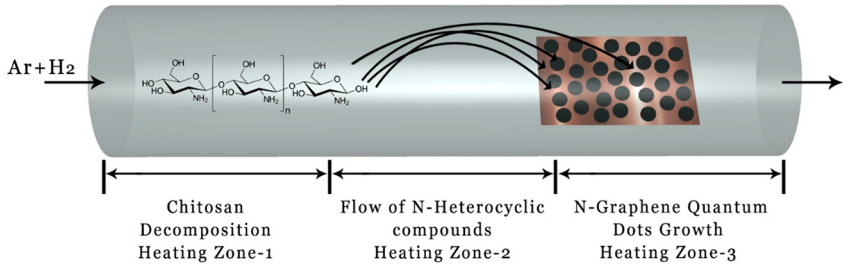

Figure 3. Schematic diagram for the synthesis of chitosan-derived N-doped graphene quantum dots N-GQDs. Reprinted with permission from ref 17. Copyright (2018) American Chemical Society.

potential for catalytic reactions attributed to different electronic structures and catalytically active sites.[26] The ability to acquire the desired N-bonding state during the process of nitrogen doping will provide a better control over the material application. However, the functions of different types of C−N bonding configurations as catalytically active sites still are a matter of debate.

PREPARATION OF CHITOSAN-BASED N-DOPED CARBON MATERIALS

Various methods were employed for the preparation of chitosan-based N-doped carbon materials. Nevertheless, controlling the position of N-doping within the carbon matrix, the density of doping and acquiring desired bonding configuration (pyridinic-N, pyrrolic-N, graphitic-N, and aminic-N) remain a significant challenge.[27] Herein, this Perspective summarizes the state of the art methods for the synthesis of chitosan-based N-doped carbon materials considering the controlling parameters that govern the properties of the resulting chitosan-based N-doped carbon materials for their applications in electrocatalysis and photocatalysis.

These methods are generally based on two techniques: direct synthesis and a postsynthesis N-doping method.

Direct Synthesis. Direct synthesis involves the incorporation of nitrogen atoms during the synthesis of carbon materials, also known as an in situ method. Direct synthesis is typically carried out through direct carbonization of chitosan as a nitrogen-rich carbon precursor or carbon precursors mixed with chitosan as a nitrogen dopant. Other methods used for direct synthesis of chitosan-based N-doped carbon materials include the solvo-thermal method, chemical vapor deposition (CVD) method, and arc discharge method.[25]

Chemical Vapor Deposition (CVD) Method. Chemical vapor deposition is one of the recent techniques used for the synthesis of chitosan-based N-doped carbon materials.[17] CVD involves the deposition of solid material from a vapor phase by the decomposition of a carbon precursor mixed with nitrogen-containing gas on the surface of a metal catalyst. By optimizing the reaction parameters such as substrate material, temperature, gas mixture composition, and gas flow pressure, materials with desired physicochemical properties can be prepared. The CVD method (Figure 3) has been successfully applied for the synthesis of chitosan-derived N-doped graphene quantum dots (N-GQDs). Chitosan has been used as the sole source of carbon and nitrogen, whereas copper foil was used as the substrate. The formation of N-GQDs initiated with the decomposition of chitosan via dehydration and deamination reactions.[28] As a result, different nitrogen-containing volatile compounds (acetonitrile, furan, pyrrole, pyridine, and pyrazine derivatives) were produced.[29] The further disintegration of the molecular structure of these volatile compounds follows complex mechanisms involving various chemical reactions accompanied by the generation of smaller molecular gases like HCN, C_2H_2, NH_3, CO, and CO_2. Then, the reaction proceeds with the adsorption of HCN (active species) on the copper foil. There they undergo further decomposition into carbon atoms. Subsequent nucleation of carbon atoms results in the growth of N-GQDs.[17]

Carbonization and Hydrothermal Carbonization. Carbonization is a complex pyrolytic process accompanied by condensation, isomerization, hydrogenation, and hydrogen transfer reactions and usually results in an increased elemental carbon content in the resulting carbon residue.[30] The carbonization method is widely used for the synthesis of chitosan-based N-doped carbonaceous materials. Verma and coworkers[31] reported a simple one-step method to prepare porous nitrogen-enriched carbonaceous carbon nitride catalysts (PCNx) through the carbonization of chitosan at 300 °C for 4 h under N_2 atmosphere. Additionally, a chitosan-based single layer N-doped graphene film was prepared on hydrophilic surfaces via a spin coating method followed by carbonization. In this method, graphene formation and doping of nitrogen occur simultaneously. The process involves the deposition of chitosan film on a quartz support by spin coating of an aqueous chitosan solution prepared in acetic acid (0.3 M). The deposited film was annealed at 200 °C for 2 h under an Ar atmosphere for the conformational relaxation (time required to change the conformation of a polymeric segment) of the fibrils to get superior quality (highly transparent and conductive) graphene material. Finally, carbonization of chitosan film within the temperature range of 600-800 °C results in the formation of a single layer to a few layers of N-doped graphene film.[32]

Graphene-like nitrogen-doped (N-doped) carbon nanosheets (NCN) were also synthesized from carbonization of chitosan and urea.[14] At lower temperature, graphitic carbon nitride g-C_3N_4 is produced from the pyrolytic breakdown of urea that served as a source of additional nitrogen and a structure-directing agent for the formation of carbon nanosheets at higher temperature. Moreover, it is also responsible for the homogeneous distribution of nitrogen within the graphene sheets and formation of graphitic and pyridinic bonding configurations.[14] The preparation of chitosan-based NCN involved the formation of a semitransparent homogeneous gel from an acetic acid/water solution (5 wt %) of chitosan and urea. The gel obtained undergoes freeze-drying followed by carbonization at 1000 °C for 5 h under an Ar flow. The process of NCN formation initiated with the condensation of urea into g-C_3N_4 and carbonization of chitosan into amorphous carbon at lower temperature (~500 °C). Meanwhile, NH_3 produced from the urea degradation resulted in the doping of nitrogen within the

https://dx.doi.org/10.1021/acssuschemeng.9b07522
ACS Sustainable Chem. Eng. 2020, 8, 4708−4727

carbon matrix. An increase in temperature (~700 °C) triggered crystallization in an amorphous carbon along with the formation of N-containing species (NH_3, $C_2N_2^+$, $C_3N_2^+$, and $C_3N_3^+$) due to the decomposition of g-C_3N_4. This step lead to the formation of multilayered graphite accompanied by the doping of nitrogen. When a temperature of 1000 °C is reached, doped nitrogen species (NH_3, $C_2N_2^+$, $C_3N_2^+$, and $C_3N_3^+$) acquired a stable state, and residual amorphous carbon transformed to graphene layers.[14]

Moreover, chitosan-derived N-doped mesoporous carbon nanosheets have also been prepared by the carbonization of chitosan and melamine (as an additional source of nitrogen) preceded by lyophilization (freeze-drying). A two-step carbonization method was employed, and initially precursors were carbonized at a temperature of 400 °C with a holding time of 30 min. Afterward, the pyrolyzed material was further carbonized up to 700 °C. Melamine exhibits 3D monoclinic structures comparable with g-C_3N_4 that assist the doping of nitrogen during its decomposition.[28]

In order to prepare highly porous N-doped carbon materials, the process of carbonization has been assisted by chemical activation. Direct carbonization incorporates nitrogen within the carbon structure, whereas chemical activation helps to increase the specific surface area of the N-doped carbon materials.[33] Highly porous N-doped activated carbon has been produced through carbonization of *Arundo donax* and chitosan using $ZnCl_2$ as an activating agent. The mixture containing precursors and an activating agent was carbonized within the temperature range of 500−700 °C for 2 h under N_2 flow to synthesize N-doped activated carbon. $ZnCl_2$ as an activating agent successfully developed porous channels within N-doped activated biocarbons. Moreover, it has been reported that carbonization temperature can be optimized to get the high specific surface area of activated biocarbon. It has been observed that N-doped activated biocarbons prepared at 500 °C exhibited higher specific surface area and pore volume as compared to other biocarbons prepared at 600 and 700 °C. This is due to the shrinkage of the carbon structure at higher temperature due to the extremely dehydrating nature of $ZnCl_2$. The textural characteristics and nitrogen content of the N-doped activated biocarbons are affected also by the ratio of precursors and activating agent, in addition to the carbonization temperature. An increase in the amount of activating agent (0-3 mass ratio) results in an increase in the specific surface area of N-doped activated biocarbon at a given temperature (500, 600, and 700 °C). This is due to a property of $ZnCl_2$ that penetrates deeper and causes hydrolysis of the biocarbon accompanied by the production of volatiles that are responsible for the high specific surface area and porosity of N-doped activated biocarbon.[34] K_2CO_3 has also been applied as an activating agent for the carbonization of chitosan to prepare N-doped microporous carbons. In order to tune the textural properties of the material, carbonization has been carried out within the temperature range from 600 to 800 °C for 1 h under an Ar atmosphere at different K_2CO_3/Chitosan mass ratios (1 and 2). The highest specific surface area (2569 $m^2\ g^{-1}$) of N-doped microporous carbons was obtained at 800 °C at a lower (1) K_2CO_3/Chitosan mass ratio.[35]

Moreover, chitosan has also been used as a functionalizing and N-doping agent to prepare N-doped graphene aerogels (NGAs). The procedure involves the dispersion of graphene in deionized water through ultrasonication (3 h) followed by the addition of chitosan. The resulting suspension was stirred at room temperature, then heated at 90 °C for 6 h. Afterward, the obtained hydrogels were washed with alcohol and acetone and dried with the help of supercritical CO_2 to form N-doped graphene oxide aerogels. Finally, N-doped graphene oxide aerogels were thermally treated (3 h) at 900 °C (5 °C/min) under a N_2 flow to get N-doped graphene aerogels. It has been observed that by optimizing the carbonization temperature (800, 900, and 1000 °C) the porous structure of the aerogels could be improved. NGAs prepared at 900 °C exhibited higher specific surface area and pore volume compared to the aerogels prepared at 800 and 1000 °C.[15]

Chitosan has also been utilized to control the volume expansion and conduction behavior of silicon material. Chitosan-derived N-doped carbon-coated milled silicon particles (N-C@m-Si) were prepared through a hydrothermal carbonization technique succeeded by simple carbonization. Prior to hydrothermal treatment, Si was ball milled (24 h) to decrease the particle size. For hydrothermal treatment, a suspension of chitosan and milled Si (m-Si) nanoparticles (1:3 by mass) were prepared in an acetic acid solution. The suspension was stirred continuously until a homogeneous solution was formed. During this process, chitosan adsorption occurred on the m-Si nanoparticle surface via intermolecular hydrogen bonding. The solution obtained underwent hydrothermal treatment at 180 °C for 12 h. The material produced through hydrothermal treatment was washed with water and ethanol and dried at 80 °C for 12 h. Finally, the composite produced was carbonized at 500 °C (10 °C/min) for 2 h (Figure 4).[36] Furthermore, the prepared N-C@m-Si was used as an

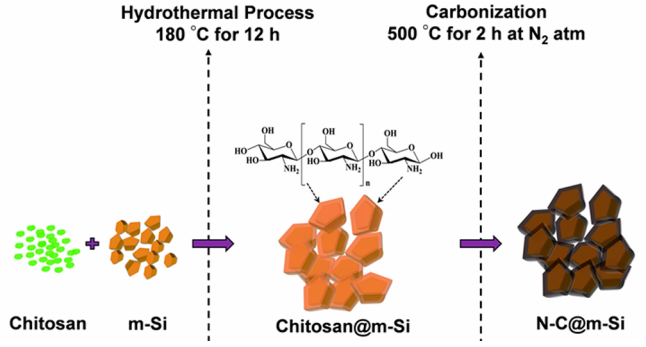

Figure 4. Preparation process of chitosan-derived N-doped carbon-coated milled silicon particles (N-C@m-Si) electrode materials. Reprinted in part with permission from ref 36. Copyright (2019) Springer Nature.

active material to prepare an anode electrode for lithium ion batteries. N-C@m-Si, polyvinylidene difluoride (PVDF), and Super P (carbon black) were used at a ratio of 80:10:10 by mass. N-Methyl pyrrolidone (NMP) was added in the mixture to form a slurry, whereas PVDF was used as the binder and Super P acted as a conductive agent. Afterward, a thin copper foil was coated with a prepared slurry and dried in air for 24 h. Finally, the prepared sample was vacuum-dried at 120 °C for 5 h.[36]

A two-step approach has also been used for the synthesis of N-doped graphitic carbon nanoparticles (N-g-CNPs) from chitosan. Here, in the first step, N-doped carbon nanoparticles (N-CNPs) have been prepared via hydrothermal carbonization of chitosan at a temperature of 180 °C for 12 h. Afterward, N-doped graphitic carbon nanoparticles (N-g-CNPs) were prepared by the pyrolysis of N-CNPs at 900 °C for 4 h. The N-CNPs (30−40 nm) obtained through hydrothermal carbon-

https://dx.doi.org/10.1021/acssuschemeng.9b07522
ACS Sustainable Chem. Eng. 2020, 8, 4708−4727

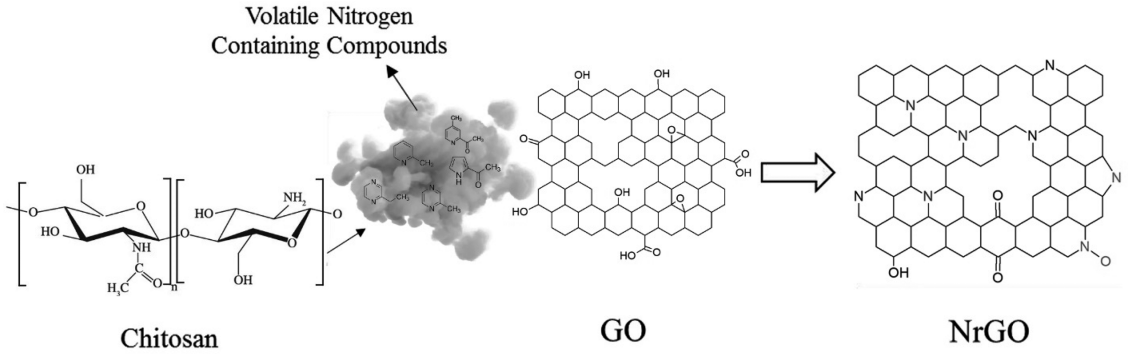

Figure 5. Synthesis of N-doped reduced graphene oxide (NrGO) using chitosan. Adapted with permission from ref 45. Copyright (2017) Elsevier.

ization were amorphous in nature. Subsequent pyrolysis at 900 °C results in the conversion of amorphous N-CNPs to N-g-CNPs. Sulfur−nitrogen-codoped graphitic carbon nanoparticles were also synthesized by adding a certain amount of powdered sulfur during hydrothermal carbonization.[16] In addition, hydrothermal carbonization following simple carbonization has also been employed to prepare chitosan-based metal-containing composites such as a N-doped carbon-coated $CoSnO_3$ composite ($CoSnO_3$@N-C). The process for the synthesis of $CoSnO_3$@N-C begins with the hydrothermal treatment of carboxylated chitosan with amorphous $CoSnO_3$ at 180 °C for 12 h. The material obtained was further calcined at 500 °C for 4 h under Ar flow. Finally, the composite-obtained $CoSnO_3$@N-C exhibited cluster-like morphology where $CoSnO_3$ particles were coated with carbon particles.[37]

Solvothermal Method. The solvothermal method is quite similar to the hydrothermal method, with the exception of the solvent used. During the solvothermal method, a chemical reaction occurred in an organic solvent instead of water at a temperature above the boiling point of the solvent. These conditions speed up the reaction between the solid species and the organic solvent. Photocatalytically active (visible light) carbon-coated N-doped TiO_2 nanostructures (CTS-TiO_2) have been prepared by a single step solvothermal technique. For this, chitosan has been used as carbon as well as a nitrogen source. The chemical reaction proceeds with the formation of a suspension of chitosan and titania precursor (titanium(IV) isopropoxide) in the mixture of ethanol and glacial acetic acid in a sealed vessel. The resulting suspension underwent solvothermal treatment at 180 °C for 12 h to obtain CTS-TiO_2.[38]

Solvent Evaporation/Solution Cast Method. The solvent evaporation method is widely used for the preparation of polymeric materials. This technique involves the dispersion of the polymer in the solvent through high-speed homogenization, ultrasonication, or continuous stirring followed by evaporation of the solvent.[39] N-doped carbon material has been prepared from chitosan via a solvent evaporation-induced gelation technique. The process involves the mixing of chitosan and Vulcan-XC 72 carbon black in ethanoic acid. Afterward, the mixture was continuously stirred and dispersed through ultrasonication in order to form a homogeneous ink. Subsequently, gelation was induced via a solvent evaporation at 50 °C that results in the formation of xerogel. Finally, the prepared xerogel was thermally treated at 900 °C for 1 h under a N_2 flow to form a chitosan-based N-doped carbon material. The obtained N-doped carbon material has been used as a catalyst support for the preparation of nanosized platinum electrocatalysts via a microwave-assisted polyol process. During the synthesis, a chitosan-derived N-doped carbon material was dispersed in ethylene glycol through ultrasonication. Subsequently, a precursor of platinum was added, and then, the pH of the mixture was adjusted to 11 by adding a 0.1 M NaOH solution. Later, the whole mixture was irradiated with microwaves (800 W) for 90 s to obtain platinum supported on N-doped carbon materials.[40] Furthermore, a Fe_3O_4/multiwalled carbon nanotubes/chitosan nanocomposite Fe_3O_4/chitosan has been prepared through the solvent evaporation method by varying the concentration of Fe_3O_4 and MWCNTs. Fe_3O_4 and MWCNTs were dispersed in water through ultrasonication (1 h), followed by the addition of chitosan and ethanoic acid. The resulting mixture was stirred for 3 h and subsequently underwent ultrasonication for 30 min. Afterward, the solution was degassed and dried at 60 °C to form a nanocomposite film with an average diameter of 0.04 mm.[41] Additionally, graphene/chitosan and cryomilled graphene/chitosan nanocomposite films have also been prepared following the same method with some modification in the stirring duration (3 h) and temperature (80 °C) used for drying.[42]

Nafion/carbon-coated iron nanoparticles-chitosan (CCINPs-CS) composite film-modified electrodes have been prepared through a solution casting method. Prior to casting, a CCINPs-CS suspension has been prepared by dispersing carbon-coated iron nanoparticles (CCINPs) into a chitosan solution via ultrasonication (30 min). Chitosan aids the formation of a stable and homogeneous suspension. Then, a drop of prepared suspension was cast on the surface of a glassy carbon electrode (GCE). Later, the GCE was coated with a Nafion solution and left to dry in air for 4 h to obtain a Nafion/CCINPs-CS composite film modified electrode.[43]

Postsynthesis N-Doping. Postsynthesis N-doping methods involve the introduction of nitrogen atoms into the prepared carbon material through reaction with nitrogen-containing precursors such as N_2, NH_3, and N_2H_4. Postsynthesis nitrogen doping is carried out in several ways such as thermal treatment, plasma treatment, and N_2H_4 treatment. The postdoping method results in surface functionalization of the carbon materials without changing the properties of the bulk material, whereas the direct synthesis allows the homogeneous distribution of nitrogen atoms within the carbon matrix.

Plasma Treatment. Plasma treatment is a state of the art technique for the surface modification of carbon material that is applied for the doping of nitrogen atoms and nitrogen-containing groups within the carbon matrix. During nitrogen plasma treatment, carbon atoms are partially substituted with nitrogen atoms. Wang and coworkers[44] reported N-doped graphene preparation via nitrogen plasma treatment of chemi-

https://dx.doi.org/10.1021/acssuschemeng.9b07522
ACS Sustainable Chem. Eng. 2020, 8, 4708−4727

cally synthesized graphene. Prior to plasma treatment, a graphene−chitosan dispersion (0.5 wt % with 2% acetic acid) was coated on the GCE surface and subsequently dried. Afterward the GCE was exposed to a nitrogen plasma environment at a pressure of 750 mTorr and plasma power of 100 W. In order to optimize the atomic percentage of N-doping, plasma exposure time was varied between 20 and 100 min.[44] It has been found that by optimizing the exposure time and plasma strength the nitrogen content (3−8.5 atom %) in the carbon materials can possibly be controlled.[25]

CVD-Assisted Postdoping. N-doped reduced graphene oxide (NrGO) was prepared via CVD-assisted postdoping of graphene oxide (GO) through volatile nitrogen-containing heterocyclic compounds produced through the thermal degradation of chitosan (Figure 5). In a typical experiment, chitosan (300 mg) and graphene oxide (15 mg) were placed far apart in a quartz tube (length, 15 cm; diameter, 8 mm) to avoid the chance of physical mixing. The quartz tube with a precursor and N-doping agent was placed in a furnace kept at atmospheric pressure under an argon atmosphere (20 mL/min) and annealed for 1 h at different temperatures (300, 450, and 600 °C) to optimize the N content and C/O ratio.[45]

During the process of annealing, chitosan underwent homolytic bond cleavage (generating radicals) and immediately formed new bonds through cross-linking reactions. Subsequent bond cleavage and cross-linking reactions produced volatile nitrogen-containing heterocyclic compounds (pyrazines, pyridines, pyrroles, and furans),[46,28] which were transferred via an Ar flow toward graphene oxide. As a result of the interaction of volatile nitrogen-containing heterocyclic compounds with graphene oxide and simultaneous reduction, NrGO was prepared. Moreover, it has been observed that among the tested temperature, the optimum CVD temperature was 450 °C with the highest content of N-doping (4.3 atom %) and maximum C/O ratio (16).[45]

CHARACTERIZATION OF CHITOSAN-BASED N-DOPED CARBON MATERIALS

Characterization of chitosan-based N-doped carbon materials is crucial to understand the bonding nature, C−N bonding configuration, structure, surface morphology (microtexture and nanotexture), and physicochemical properties for their electrocatalytic and photocatalytic applications. Moreover, it will also be helpful in designing new materials, improving their properties, and gaining insight into the synthesis method-dependent material properties.[47]

X-ray Photoelectron Spectroscopy (XPS) Technique. XPS is the quantitative technique to determine the surface content of doped nitrogen in chitosan-based N-doped carbon materials. Moreover, it gives information of whether the doped nitrogen atom is substituted for a backbone carbon atom or part of functional moieties.[47] In the XPS spectrum, the peak intensity ratios of N 1s and C 1s are used to calculate the surface nitrogen content, whereas by the deconvolution of the N 1s spectrum the C−N bonding configuration in chitosan-based N-doped carbon materials can be studied. Guo and coworkers[48] observed (Figure 6) four types of C−N bonding configurations in chitosan-based N-doped carbon nanoflowers, i.e., pyridinic-N, pyrrolic-N, graphitic-N, and N−O at the binding energies of 398.4, 399.9, 400.8, and 401.8 eV, respectively.[48]

However, slight variations in the peak positions of nitrogen species have been observed in different chitosan-based N-doped carbon materials.[49] Moreover, it has been observed that C−N bonding configuration and nitrogen content are greatly influenced by preparation conditions such as temperature treatment and changing precursor amount. Generally high temperature treatment (700−1000 °C) favors the formation of graphitic-N[14,48] that is favorable for electrocatalytic[48] and photocatalytic applications.

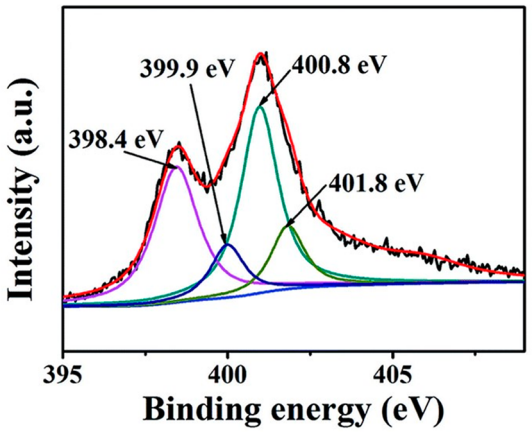

Figure 6. High resolution XPS of N 1s peaks for a chitosan-based N-doped carbon nanoflower. Reprinted with permission from ref 48. Copyright (2017) Royal Society of Chemistry.

UV−Vis Diffuse Reflectance Spectroscopy (UV−vis DRS). UV−vis DRS is a very useful technique to study the optical absorption properties of the chitosan-based N-doped carbon materials. Light absorption properties of the chitosan-based N-doped carbon materials are very crucial for their photocatalytic application. Liu and coworkers[50] observed that the color of C self-doped g-C_3N_4 changes from yellow to black by increasing the chitosan content during synthesis. Interestingly, the light absorption ability of pristine g-C_3N_4 and C self-doped g-C_3N_4 prepared without the addition of chitosan (CCN-0) was limited up to 450 nm, whereas after chitosan addition the light absorption ability of C self-doped g-C_3N_4 at higher wavelengths has been improved. The C self-doped g-C_3N_4 optimized sample (CCN-0.2) was able to absorb light within the range of 450−700 nm. Consequently, the band gap calculated by the Kubelka−Munk function for CCN-0.2 was reduced (2.5 eV) compared to pristine g-C_3N_4 (2.7 eV) and CCN-0 (2.6 eV). The reduced band gap positively influenced the photocatalytic performance of CCN-0.2 for H_2 generation, i.e., 29.1 times (320 μmol h^{-1}) more than pristine g-C_3N_4.[50] Moreover, chitosan has been reported to increase the visible light absorption and reduce the band gap of TiO_2 in the form of a composite. TiO_2 principally absorbs UV light, whereas the introduction of chitosan in TiO_2 enhanced its visible light absorption up to 650 nm. Besides that, it reduced the band gap of the prepared TiO_2 from 3.1 to 2.8 eV.[51]

Gas Adsorption/Desorption Isotherm Measurement. The measurement and analysis of gas adsorption/desorption isotherms are of major importance for the characterization of the pore structure of chitosan-based N-doped carbon materials. Pore structure and specific surface area of the catalyst is closely linked with electrocatalytic and photocatalytic performances; therefore, N_2 adsorption and desorption isotherm measurements have been carried out for chitosan-based N-doped carbon materials. Pore structure is defined by a number of parameters, like pore size, pore volume, surface area, and pore shape.[52] It has been observed that an increase in carbonization temperature up to certain extent (600−900 °C) results in an increase in surface

https://dx.doi.org/10.1021/acssuschemeng.9b07522
ACS Sustainable Chem. Eng. 2020, 8, 4708−4727

area, mesopore volume, micropore volume, and total pore volume of chitosan-derived N-doped carbon nanoflowers. The highest surface area (907 $m^2 g^{-1}$) and pore volume (1.85 $cm^3 g^{-1}$) have been observed for the sample carbonized at 900 °C. Interestingly, the chitosan-derived N-doped carbon nanoflowers share the same trend of electrocatalytic activity as that of specific surface area and pore volume variation. Accordingly, high accessible specific surface area was attributed to be responsible for the provision of active sites.[48] Moreover, high specific surface area and porosity not only provide numerous active sites but also support electrolyte ion diffusion. Additionally, the heteroatom in the carbon material induces redistribution of charge which can accelerate electron transfer in electrocatalytic reactions.[53] Mesopores were found to be mainly responsible for increasing the number of available active sites, whereas macropores offer improved mass and charge transport[54] thereby making the available active site kinetically accessible during electrocatalytic reactions.[55]

A similar trend of enhanced photocatalytic activity for the degradation (96.8%) of Rhodamine B (RhB) with an increasing specific surface area (189 $m^2 g^{-1}$) has been observed for a chitosan-derived N-doped, carbon species-decorated TiO_2 composite sample that might be attributed to the greater number of available catalytic sites,[56] whereas pristine titania exhibited a smaller specific surface area (129 $m^2 g^{-1}$) and lower degradation of RhB (38.2%).[51]

Raman Spectroscopy. Raman spectroscopy is a useful technique for the characterization of the structure and electronic properties of chitosan-based N-doped carbon materials, especially graphene-like materials.[25] Chitosan-derived N-doped graphene showed characteristic "G" and "D" Raman bands at 1580 and 1380 cm^{-1}, respectively. The G-band corresponds to C−C stretching in the graphene material due to a sp^2 carbon network, whereas the D-band is characteristic of a disordered structure of graphene having low crystallinity.[57] The D-band is also due to the existence of a N atom that acts as a defect in the graphene layers.[58] Moreover, the Raman intensity ratio (I_D/I_G) has been used as a measure of graphitization which is inversely related to the in-plane crystallite size.[59] As the I_D/I_G value increases, the degree of graphitization and crystallite size decreases. Besides that, the temperature applied for the synthesis of materials also plays a crucial role in determining the degree of graphitization and controlling the defects. Chitosan-based N-doped carbon nanosheets (NCN) prepared at different temperatures (given as °C in sample names), i.e., NCN-900, NCN-1000, and NCN-1100, showed a decrease in I_D/I_G values (1.126, 1.038, and 0.995, respectively,).[14] The higher value of I_D/I_G is an indication of more defects and a smaller crystallite size that is conducive for electrocatalytic activity of NCN.[60]

Photoluminescence (PL) Spectroscopy. Photoluminescence (PL) spectroscopy is commonly used to study the irradiative recombination of photogenerated charge carriers. It provides an insight into optical and charge transfer properties of the N-doped carbon materials. Chitosan introduced in g-C_3N_4 for the partial substitution of N with C in the as-prepared sample CCN-1 (1 corresponds to the mass percentage of chitosan to melamine) enhanced the charge separation by reducing the recombination of charge carriers. It can be seen in Figure 7 that pristine g-C_3N_4 exhibited a high intensity PL peak at 470 nm that suggests fast electron−hole recombination,[61] whereas CCN-1 showed a substantial drop in the PL peak intensity that signifies reduction in recombination of charge carriers. This decrease in PL peak intensity is attributed to the presence of a carbon bridge between heptazine units that allows charge transfer between heptazine rings.[62] This accelerated charge migration has also been observed for ternary catalysts based on amino-functionalized carbon quantum dots (chitosan-derived), g-C_3N_4 nanosheets, and a cobalt complex. The reduced recombination of charge carrier for the ternary catalyst compared to pristine g-C_3N_4 is due to the formation of amide bonds within the catalyst which assist charge transformation that is beneficial for the photocatalytic activity of catalyst.[63]

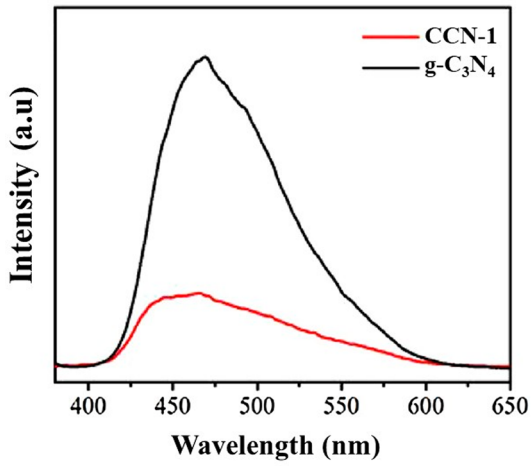

Figure 7. Photoluminescence spectra of pristine g-C_3N_4 and CCN-1. Reprinted with permission from ref 62. Copyright (2018) Elsevier.

X-ray Diffraction (XRD) Analysis. The XRD technique is a useful technique to study the crystallinity and degree of graphitization in chitosan-based N-doped carbon materials. XRD analysis confirms the graphitization in a chitosan-based N-doped carbon nanoflower by the presence of two broad diffraction peaks at 2θ values of 25.2° and 42.5° corresponding to the (002) and (100) planes of graphite.[48] The broad XRD reflexes refer to the disordered stacking of graphene nanosheets which have also been observed in chitosan-functionalized N-doped graphene aerogels.[15] Moreover, a small shift in the (002) reflection to a lower angle has occurred in chitosan-based N-doped graphitic carbon that is due to the increased interlayer spacing caused by doping.[64,16]

APPLICATIONS OF CHITOSAN-BASED N-DOPED CARBON MATERIALS

Novel carbonaceous materials with distinct morphologies (like carbon nanotubes, nanofibers nanodiamonds, nanospheres, and quantum dots) and composition (nitrogen-, phosphorus-, and boron-doped carbons) have significant potential for catalytic applications. Carbon-based materials can be used as a catalyst as well as a catalyst support for enzymatic and chemical reactions.[65] The peculiar physicochemical properties of carbon-based materials such as high specific surface area and porosity, low density, hydrophobicity, greater electron conductivity, chemical stability, and resistance to acidic and basic media make them suitable candidates for catalytic applications.[66,67] N-doped carbons materials and metal-supported N-doped carbon materials have recently gained much attention because they exhibited high electrocatalytic[68] and photocatalytic activity. In the context of electrocatalytic application, lignin- and chitin-derived N-doped carbon materials showed exceptional performance as electrocatalysts for the oxygen reduction reaction.[69,70] Furthermore, other biomass-derived materials such as cellulose-

https://dx.doi.org/10.1021/acssuschemeng.9b07522
ACS Sustainable Chem. Eng. 2020, 8, 4708−4727

and biochar-derived N-doped carbon materials proved to be effective photocatalysts for pollutant degradation[71,72] Herein, we focus on recent progress in the potential application of chitosan-based N-doped carbon materials for electrocatalysis and photocatalysis.

Electrocatalytic Applications. *Oxygen Reduction Reaction (ORR).* Multiple catalytic and electrocatalytic methods are required to meet the demands for sustainable technologies in the field of energy conversion and storage. Electrocatalysis plays a crucial role in fuel cells and metal−air batteries for the oxygen reduction reaction (ORR) occurring at the cathode. However, the slow kinetics of the oxygen reduction reaction compared to metal oxidation limits the inclusive power capabilities of these electrochemical devices. Currently, platinum is considered to be the most active electrocatalyst for the ORR in acidic as well as in basic conditions.[73] However, the high cost of platinum metal and its poisoning via CO impedes the large-scale application of these devices. Therefore, there is a need to develop a cost-effective, sustainable electrocatalyst for the oxygen reduction reaction.[20] In order to address this issue, metal-free carbon-based materials (graphite, graphene, carbon nanotubes) have increasingly been used to prepare electrocatalysts for the ORR in fuel cells due to their high conductivity, high mechanochemical stability, and high specific surface area.[74] N-doping of carbon materials modifies their electronic properties (specifically carrier transport ability), making them principally applicable for the electrocatalytic ORR in electrochemical devices.[20] For example, N-doped carbon dots-deposited graphene oxide (N-Cdots/GO) hybrids have shown remarkable electrocatalytic efficiency for the ORR in an O_2-saturated 0.1 M KOH solution at 1000 rpm. N-Cdots/GO exhibited an onset potential of 0.13 V vs Ag|AgCl and high kinetic current density of up to 18.4 mA cm^{-2} at −0.70 V, which is comparable to the commercial Pt/C catalyst (~0.03 V and ~25.8 mA cm^{-2}), respectively.[75]

The enhanced electrocatalytic activity of N-doped carbon materials for the ORR is attributed to the redistribution of the charge density of adjacent C atoms due to the difference of electronegativity between carbon and nitrogen atoms.[76] The change in charge density alters the chemisorption mode of the O_2 molecule from end-on adsorption to side-on adsorption which weaks the O−O bond and favors the ORR. In addition, the charge transfer induced by N-doping (pyridinic-N) imparts Lewis basicity to the carbon atom next to pyridinic-N and creates an ORR active site[77,78] Nevertheless, it is still challenging to identify the active sites and the heteroatom content in the carbon basal plane and develop a definite relationship between the C−N bonding configuration and electrocatalytic activity.

Guo and coworkers[78] reported a plausible mechanism of the ORR on a N-doped carbon catalyst (Figure 8). Here, the reaction begins with the adsorption of an O_2 molecule (A in Figure 8) on the active site (carbon atom next to pyridinic-N) followed by protonation (C in Figure 8). At this stage, the ORR follows either a two-electron process (two-steps) or four-electron process (single-step). During the four-electron process, the other two protons attach to the two oxygen atoms, resulting in breakage of the O−OH bond and generating hydroxyl species (D in Figure 8). The fourth proton then reacts with the adsorbed hydroxyl and forms water (E in Figure 8), whereas during the two-electron process the adsorbed OOH reacts with a proton and forms H_2O_2 (F in Figure 8). Finally, the H_2O_2 formed readsorbed and after reacting with two protons formed water.[78]

Chitosan as N-containing biomass has received much attention recently for the preparation of N-doped carbon

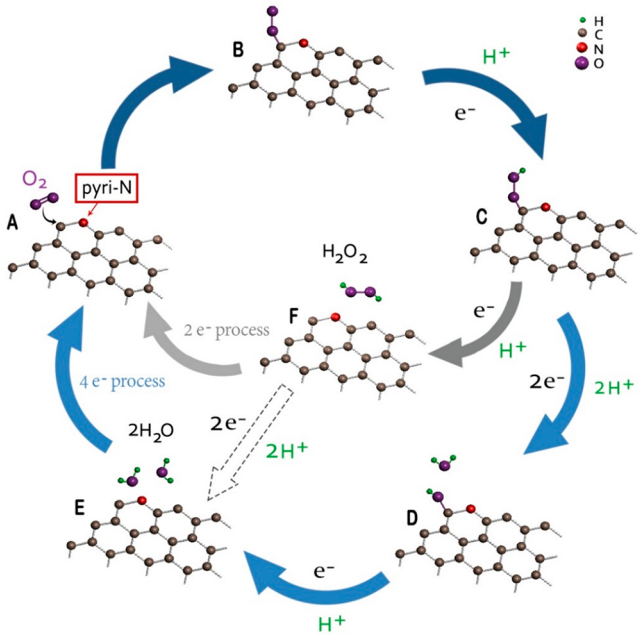

Figure 8. Schematic pathway for oxygen reduction reaction on N-doped carbon materials. Reprinted with permission from ref 78. Copyright (2016) The American Association for the Advancement of Science.

materials for high efficiency ORR electrocatalysts. Chitosan and amino-modified urchin-like hierarchical silica spheres nanoparticles (UHSSs-NH_2)-derived N-doped carbon nanoflowers were investigated for the ORR electrocatalytic activity via linear sweep cyclic voltammetry curves (LSV) using 0.1 M KOH at 1600 rpm and a scan rate of 10 mV s^{-1}. 3D hierarchical NCNF electrocatalysts prepared at 800 °C carbonization temperature in different mass ratios of chitosan and UHSSs-NH_2, i.e., 1:1 (NCNF1-800), 2:1 (NCNF2-800), and 3:1 (NCNF3-800), have shown different activities for the electrocatalytic ORR (Figure 9a). NCNF2-800 showed higher current density and more positive onset potential (0.923 V vs RHE) in comparison with NCNF1-800 and NCNF3-800 (0.906 and 0.903 V vs RHE, respectively). The higher activity of NCNF2-800 (entry 1, Table 1) was attributed to its greater specific surface area (873 m^2 g^{-1}) offering more active sites and generating a larger catalytic current density as compared to NCNF1-800 and NCNF3-800 (686 and 482 m^2 g^{-1}, respectively). Moreover, NCNF2-800 contained a higher content of doped nitrogen (7.8 atom %) relative to NCNF1-800 (4.5 atom %) and NCNF3-800 (6.9 atom %) that provides effective intrinsic activity. However, the activity of NCNF2-800 is slightly lower than that of a commercial 20 wt % Pt/Carbon catalyst.[48]

Additionally, a series of catalysts were prepared treating NCNF2 at different carbonization temperatures (NCNF2-600, NCNF2-700, NCNF2-750, NCNF2-800, NCNF2-900, and NCNF2-1000) to evaluate the effect of annealing temperature on the ORR activity. The LSV curves showed more positive onset potential and current density for the ORR activity with increasing annealing temperatures except for NCNF2-1000 (Figure 9b). A similar trend has been observed for the ORR activity through the cyclic voltammetry (CV) technique. The most positive peak potential of 0.86 V (vs RHE) with the highest reaction current of 317 mA after background current correction was observed for NCNF2-900. Interestingly, NCNF2-900 and NCNF2-1000 showed slightly higher activity than the

https://dx.doi.org/10.1021/acssuschemeng.9b07522
ACS Sustainable Chem. Eng. 2020, 8, 4708−4727

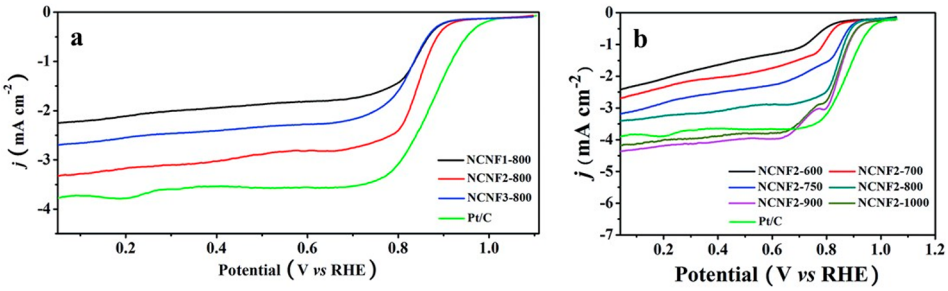

Figure 9. (a) Linear sweep voltammetry (LSV) curves at 1600 rpm and 10 mV s^{-1} of NCNF800-1, NCNF800-2, NCNF800-3, and 20% Pt/C catalysts in 0.1 M KOH. (b) LSV curves of NCNF600-1, NCNF700-2, NCNF750-2, NCNF800-1, NCNF900-2, NCNF1000-2, and 20% Pt/C catalysts. Reprinted with permission from ref 48. Copyright (2017) Royal Society of Chemistry.

commercial Pt/carbon catalyst with a slightly negative onset potential for the ORR and larger current reactions. Furthermore, the higher electrochemical activity of NCNF2-900 was attributed to its higher specific surface area (907 m^2 g^{-1}) and pore volume (1.85 cm^3 g^{-1}) offering more catalytic active sites and allowing a faster diffusion and better permeation of electrolyte ions as well as generating a larger catalytic current density.[48]

Nevertheless, the utmost concern associated with the performances of electrocatalysts for the ORR is their low activity compared to Pt/C and low stability in acidic medium. Multiwalled carbon nanotubes (MWCNTs) being highly conductive in nature can be employed for the electrocatalytic ORR by facilitating the electrochemical electron transfer processes. However, pristine MWCNTs have shown low activity for the ORR attributed to the absence of active sites. Coating of MWCNTs with chitosan-based N-doped carbon via hydrothermal carbonization with subsequent annealing (1000 °C) is one of the effective ways to enhance the activity of MWCNTs for the ORR and their stability in alkaline as well as acidic media. According to the LSV curves, the carbon−carbon nanocomposites (denoted as NC-CNT-1000) showed an onset potential below 0.6 V (vs RHE), which is more negative than Pt/C in an alkaline medium (0.10 M KOH solution) at a rotation rate of 1600 rpm and with a scan rate of 10 mV. However, NC-CNT-1000 showed better activity with a limiting current density of approximately 6.9 mA cm^{-2} than Pt/C (~6.7 mA cm^{-2}).[79]

Moreover, NC-CNT-1000 has also shown significant activity in an acidic medium (O_2-saturated 0.10 M $HClO_4$ solution at a rotation rate of 1600 rpm and with the scan rate of 10.0 mV s^{-1}), although the onset potential of NC-CNT-1000 is more negative than for Pt/C. However, the current density exhibited by NC-CNT-1000 (~6 mA cm^{-2}) was quite comparable with commercial Pt/C (~7 mA cm^{-2}) at approximately 0.1 V. The ORR efficiency of a electrocatalyst is driven by a number of crucial factors such as the inherent nature of the active sites that is governed by the interaction of the catalyst components and its chemical composition. Besides that, the number of active sites directly in contact with the electrolyte and present in micropores also plays a significant role in the ORR performance. Micropores can generally electro-adsorb hydrated ions at a low concentration-dependent rate, whereas a pore size greater than 0.5 nm may also be electrochemically accessible but contribute little to the electro-active surface area.[80] In contrast, mesopores and the crystallinity facilitate the electron and mass transport abilities of the catalyst, contributing to an increase in the number of active sites.[81,82] The better performance of NC-CNT-1000 in the electrocatalytic ORR even in acidic media is attributed to synergy between the framework of MWCNTs and the coating of N-doped carbon (NC).[79] Chitosan is responsible for introducing the active N-site within the framework of MWCNTs. Additionally, the remaining iron carbide (entrapped inside the MWCNTs from the ferrocene thermal treatment during MWCNT synthesis) establishes linkages with graphitic carbon, thereby activating the neighboring graphitic layers and developing active sites,[83,84] whereas the iron present on the surface of NC-coated MWCNTs establishes Fe−N-C bonds that will also act as an active site for the ORR. Furthermore, NC coating supports the growth of a 3D-network structure that promotes the mass and electron transfer process. Besides that, the NC coating also serves as a protective layer by shielding the Fe-based active sites over the surface of MWCNTs from H_2O_2 poisoning (ORR by product), hence enhancing the stability and durability of the catalyst.[79]

Thus far, few studies have explored the potential of chitosan-based N-doped carbon materials for the ORR in fuel cells and other electrochemical devices. Xie and coworkers[85] designed cobalt and nitrogen-codoped carbon materials using chitosan as sustainable source of carbon and nitrogen. The ORR performance of cobalt and nitrogen-codoped carbon materials prepared at 900 °C (denoted as CoNC-900) after optimization was evaluated through linear-sweep voltammetry (LSV) curves on a rotating disk electrode (RDE) at 1600 rpm in a 0.1 M KOH solution saturated with O_2. TheCoNC-900 electrocatalysts displayed an onset potential of −0.044 V vs AglAgCl (Figure 10a) which is close to that of the state of the art Pt/Carbon commercial catalyst (−0.046 V). However, CoNC-900 showed better electrocatalytic activity with higher limiting current density (5.36 mA cm^{-2}) and more positive half-wave potential (−0.105 V) compared to the commercial Pt/Carbon catalyst (with 5.04 mA cm^{-2} current density and around −0.120 V half-wave potential). Moreover, the performance of CoNC-900 has also been compared with catalysts prepared without Co doping (NC) and prepared through mechanical mixing (M-CoNC). However, NC showed very little electrocatalytic activity, whereas M-CoNC displayed reasonable activity with an onset potential of (−0.168 V). Nevertheless, CoNC-900 showed the best electrocatalytic activity compared to other catalysts (NC, M-CoNC, and Pt/C). The maximum activity of CoNC-900 is attributed to the doping of Co and ensuing uniform Co−N−C bonds due to the strong chelating linkage between Co and $-NH_2$ groups which are attributed to play a pivotal role in electrocatalysis.[85] The carbonization temperature is a critical factor for the incorporation of nitrogen in the carbon matrix. Lower temperature results in incomplete carbonation that leads to poor conductivity and lower activity, whereas very high

https://dx.doi.org/10.1021/acssuschemeng.9b07522
ACS Sustainable Chem. Eng. 2020, 8, 4708−4727

Table 1. ORR Electrocatalytic Performance (Onset Potential, (E_{Onset}), Half-Wave Potential ($E_{1/2}$), and Limiting Current Density (J_1)) of Chitosan-Based N-Doped Carbon Materials in O_2 Saturated 0.1 M KOH Electrolyte at a Rotation Speed of 1600 rpm

Entries	Electrocatalyst	Precursors	Synthesis methods	N-doping (atom %)	Specific surface area ($m^2\ g^{-1}$)	Pore volume ($cm^3\ g^{-1}$)	Scan rate ($mv\ s^{-1}$)	E_{Onset} (V)	$E_{1/2}$ (V)	J_1 ($mA\ cm^{-2}$)	Transferred electrons (n)	ref
1	N-doped carbon nanoflower (NCNF2-800)	Chitosan	Silica template method	7.8	873	1.69	10	0.92 vs RHE	0.82[b] vs RHE	3.3[b] vs 0.1 V	3	48
2	Co and N-codoped carbon material (CoNC-900)	Chitosan and $Co(NO_3)_2$	Pyrolysis	6.5	220	NR	100	−0.044 vs Ag/AgCl	−0.105 vs Ag/AgCl	5.36 vs −0.6 V	3.9	85
3	N-doped multiwalled carbon nanotubes (NC-CNT-1000)	Chitosan and multiwalled carbon nanotubes	Hydrothermal and annealing	1.2	187	0.19	10.0	0.85[b] vs RHE	0.68[b] vs RHE	6.9[b] vs 0.2 V	3.6	79
4	N-doped carbon-Nd_2O_3 (Nd_2O_3/N-C hybrid material)	Chitosan and neodymium(III) nitrate hexahydrate	Annealing	~18	NR	NR	5	−0.04 vs SCE	~0.08 vs SCE	570 vs −0.6 V	3.9	116
5	Graphene-like N-doped carbon nanosheets (NCN)	Chitosan and urea	Pyrolysis	4.3	1510	1.32	5	−0.03 vs Ag/AgCl	−0.17[b] vs Ag/AgCl	37 vs −0.6	4	14
6	Cobalt/N-doped carbon nanotubes (Co16%- NCNT-T800)	Chitosan, urea, and cobalt(II) acetate	Annealing	7.6	337	NR[a]	10	0.92[b] vs RHE	0.83 vs RHE	6.9 vs 0.2 V	3.2	49
7	Pt/Carbon, commercial	NR	NR	NR	NR	NR	100	−0.046 vs Ag/AgCl	−0.120 vs Ag/AgCl	5.04 vs −0.6 V	3.9	85

[a]NR: not reported. [b]Data are estimated from the figures.

temperatures result in the breakage of the Co and N bond within the matrix and reduce the electrocatalytic activity of the catalyst by lowering the number of active sites.[86] Moreover, the high nitrogen content in CoNC-900 (~6.5 atom %) compared to NC (<1 atom %) and M-CoNC (~2.5 atom %) and the presence of ORR-active nitrogen species such as pyridinic-N (including Co-N_x) and graphitic-N are responsible for the better electrocatalytic activity of CoNC-900 (entry 2, Table 1).[85] A similar relationship between the optimum annealing temperature and active site density and the ORR activity has been observed by Liu and coworkers for chitosan-derived graphene-like N-doped carbon nanosheets (NCN).[14]

Additionally, the degree of graphitization is another imperative factor that controls the activity of the catalyst by reducing resistance in electron transfer. The lower efficiency of NC corresponds to the poor degree of graphitization compared to M-CoNC and CoNC-900. Furthermore, CoNC-900 exhibited much greater durability and tolerance toward methanol (2 M), showing only 8% current loss over 10 h compared to Pt/C (more than 20%) in an O_2-saturated 0.1 M KOH solution at −0.30 V and rotation rate of 1600 rpm. The electron transfer number (n) during the ORR was determined through the Koutecky−Levich (K−L) equation at various electrode potentials. It has been found that CoNC-900 followed a quasi-four-electron process (Figure 10b) with an average n value of approximately 3.98, which is appropriate for attaining high efficiency for the electrocatalytic ORR.[85]

Electrochemical activity of N-doped carbon materials is driven by various factors, like the surface area of the catalyst and nitrogen content, and these properties are largely governed by the condition used for the preparation of materials such as carbonization temperature. Thus, carbonization temperature is critical for determining the C−N bonding configuration and indirectly defines the electrocatalytic activity of the N-doped carbon materials. Graphitic-N and pyridinic-N are considered to be electrochemically active nitrogen species for the ORR.[87,88] It has also been supported by investigations on chitosan-based N-doped graphitic carbon nanoparticles (N-GCNPs) that showed superior electrocatalytic performance for the ORR than N-doped carbon nanoparticles (N-CNPs). Specifically, the LSV curves of N-GCNPs showed enhanced electrocatalytic activity compared to N-CNPs in a 0.1 M KOH solution saturated with O_2 at 1600 rpm, with an onset potential of −0.07 and −0.29 V, respectively. This was due to the presence of a high pyridinic-N content and low pyrrolic-N content (Figure 2) in N-GCNP as compared to N-CNP. Moreover, the onset potential of N-GCNPs (−0.07 V) was comparable to commercial Pt/C (−0.04 V). Although, a higher pyridinic-N content is one of the key factors responsible for the higher activity of N-GCNPs, the higher specific surface area and larger pore volume of N-GCNPs (533 and 0.65 $cm^3\ g^{-1}$, respectively) compared to NCNPs (266 and 0.36 $cm^3\ g^{-1}$, respectively) are also attributed to increase the ORR activity by assisting in mass and electron transport. The mean transferred electron number calculated from a K−L plot was 3.9 for N-GCNPs that showed the required four-electron transition for the ORR process, whereas NCNPs followed a two-electron process for the ORR.[16]

Liu and coworkers[14] have also observed that the activity and stability of chitosan-derived graphene-like N-doped carbon nanosheets (NCN) for ORR are closely related to ultrahigh specific surface area (~1510 $m^2\ g^{-1}$) and the high content of graphitic- and pyridinic-N species (2.69 and 1.20 atom %, respectively). These features impart high electronic conductivity

https://dx.doi.org/10.1021/acssuschemeng.9b07522
ACS Sustainable Chem. Eng. 2020, 8, 4708−4727

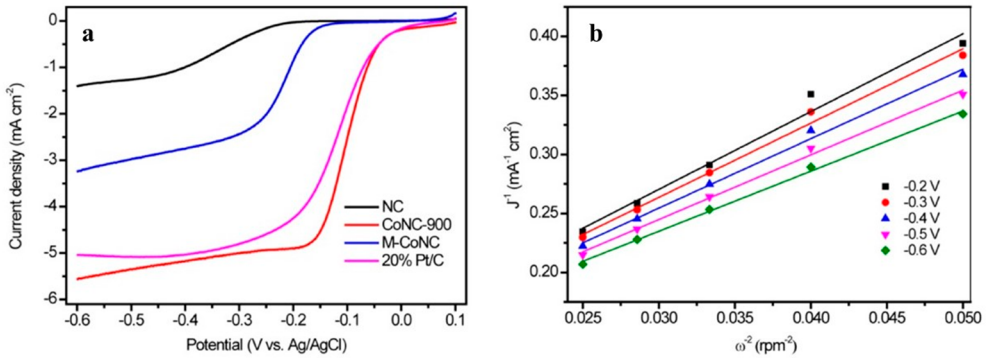

Figure 10. (a) Current density versus potential of the Co-free NC, M-CoNC, CoNC-900, and Pt/C for ORR in an O_2-saturated 0.1 M KOH electrolyte at a rotation speed of 1600 rpm. (b) K–L plots of CoNC-900 at different potentials. Reprinted with permission from ref 85. Copyright (2015) Royal Society of Chemistry.

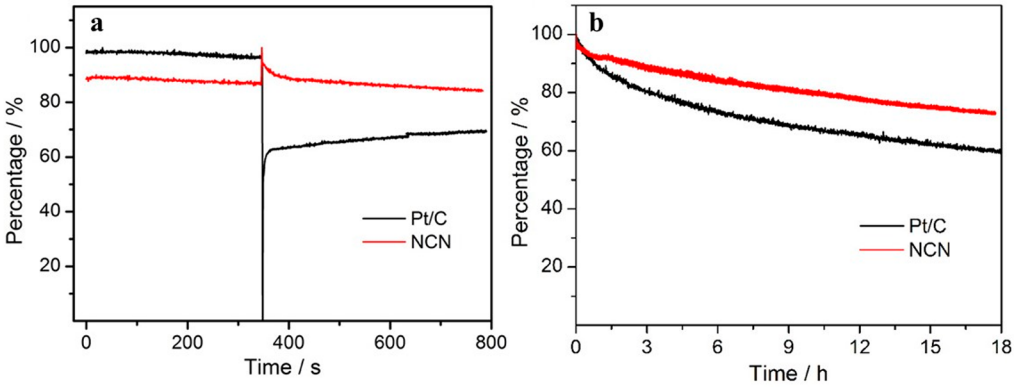

Figure 11. Chronoamperometric responses (given as percentage of current over time) of NCN and Pt/C electrodes in an O_2-saturated 0.1 M KOH electrolyte at −0.45 V with a rotational rate of 1600 rpm. Methanol (3 M) was added at around 350 s in panel (a). The ORR's response persisted for 18 h in panel (b). Reprinted with permission from ref 14. Copyright (2014). American Chemical Society.

and assist in mass transport,[81] resulting in high performance of NCN in the ORR (see entry 5, Table 1, for detailed electrocatalytic activity) in an alkaline medium (O_2-saturated 0.1 M KOH at a scan rate of 5 mV s^{-1} and a rotational speed of 1600 rpm) as determined through LSV. NCN showed onset potentials at approximately −0.03 V (vs Ag|AgCl) that is approximately 18 mV more negative than commercial Pt/C. Conversely, it showed higher (37.04 mA cm^{-2}) limiting current density than Pt/C (~23.26 mA cm^{-2}). In addition to that, it followed the desirable four-electron ORR process according to the K–L equation. Besides the better electrocatalytic activity, NCN showed superior stability in terms of methanol tolerance for the ORR, compared to Pt/C.

Chronoamperometric responses were recorded for NCN and Pt/C electrodes in a 0.1 M KOH electrolyte (O_2-saturated) at −0.45 V at a rotational rate of 1600 rpm (Figure 11a). NCN maintained a stable response after the addition of 3 M methanol at around 350 s, whereas Pt/C showed a drastic decrease in current. NCN has also exhibited better long-term stability with 27% activity loss as compared to Pt/C that showed a 41% reduction in current after 18 h (Figure 11b).[14]

Methanol Oxidation Reaction (MOR). Active and stable catalysts for the methanol electrooxidation reaction are of crucial significance for the viability of the direct methanol fuel cell (DMFC) technology at a commercial scale. Pt is used as a conventional catalyst for DMFC process. However, the high cost associated with the expensive Pt catalysts and the poisoning of Pt due to the formation of CO intermediate molecules during the methanol oxidation reaction (MOR) are key concerns associated with Pt catalysts.[89] Nitrogen doping in carbon materials aids in improved dispersion of Pt that might increase the activity of the electrocatalyst for MOR by the synergistic interaction between the carbon and Pt.[90] This synergy and enhanced activity has been observed for a chitosan-based electrocatalyst, Pt/Graphene–chitosan composite (Pt/GNs-(CS)), employed for MOR. The electrocatalytic activity of Pt/GNs(CS) was investigated through CV curves in acidic media using a (0.5 M H_2SO_4) 1 M CH_3OH solution at a scan rate of 100 mV s^{-1}. Pt/GNs(CS) showed considerably better performance for MOR than a commercial 20% Pt/C catalyst with an onset potential of 0.36 V (vs Ag|AgCl) and 0.45 V (vs Ag|AgCl), respectively. Additionally, Pt/GNs(CS) depicted a mass activity (forward peak current density) 2.3 times higher (1031 mA mg^{-1}) than Pt/C (455 mA mg^{-1}).[91] The superior performance of Pt/GNs(CS) was attributed to the improved dispersion of Pt particles and enhanced interaction between Pt and carbon materials by Wang and coworkers.[91] However, this is not supported with additional data. Besides that, chitosan also prevents the irreversible aggregation of Pt/GNs(CS) that sustains the activity of the catalyst. Furthermore, electrochemical impedance spectroscopy (EIS) analysis indicated that the higher electrocatalytic activity of Pt/GNs(CS) may be attributed to its improved electron transfer ability. Pt/GNs(CS) depicted a reduced charge transfer resistance and faster reaction rate for MOR compared to Pt/C determined through Nyquist plots of EIS for methanol electrooxidation (1 M CH_3OH + 0.5

https://dx.doi.org/10.1021/acssuschemeng.9b07522
ACS Sustainable Chem. Eng. 2020, 8, 4708–4727

M H_2SO_4) at 0.5 V. Moreover, Pt/GNs(CS) showed enhanced tolerance for CO poisoning with a lower CO oxidation peak potential (0.64 V vs AglAgCl) than Pt/C (0.72 V vs AglAgCl). The better CO poisoning tolerance of Pt/GNs(CS) attributed to the intricate interaction between the Pt particles and nitrogen-containing functional groups of chitosan.[92] This interaction modulates the electronic structure of Pt particles that led to the reduction in CO adsorption on active sites by decreasing the binding energy of the Pt−CO bond. Therefore, CO oxidation on Pt/GNs(CS) is more favorable than over Pt/C.[91]

Zhou et al.[93] proposed the underlying reason for enhanced electrocatalytic activity of N-doped carbons for MOR. N-doping into carbon materials resulted in the reduction of oxygenated functional groups that leads to an improved tolerance toward oxidation (carbon corrosion processes during fuel cell operation). Furthermore, it modifies the electronic structure and results in an increase in specific capacitance and binding energies. The higher specific capacitance is an indication of higher charged species near the surface that could possibly participate in a cocatalyst-type reaction mechanism on Pt/N-doped carbon, whereas the higher binding energies reduced the interaction between Pt nanoparticles and MOR intermediates responsible for the poisoning of the catalyst.[93] Additionally, the C−N defects also help in the adsorption of oxygenated intermediates at the catalyst particle interface and inhibits the blocking of active sites during the MOR (Figure 12) and are thus increasing the electrochemical activity.

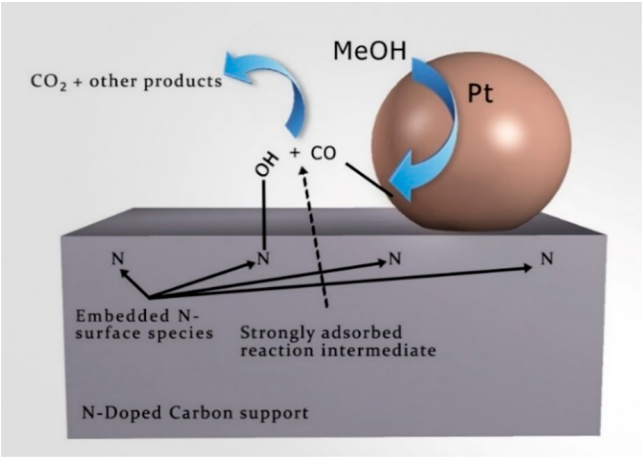

Figure 12. Schematic of possible methanol oxidation reaction (MOR) mechanisms involving oxophilic C−N defects near a C/Pt catalyst particle interface. Reprinted with permission from ref 93. Copyright (2010). Royal Society of Chemistry.

Besides that, N-doping in carbon supports assists in developing strong metal−support interaction at the interface by donating charge to neighboring atoms.[94] It has been observed that C−N defects not only serve as nucleation sites for Pt nanoparticles but also assist in their uniform dispersion by inhibiting agglomeration, thereby enhancing the electrocatalytic activity.[93] Nevertheless, the role of the C−N bonding configuration in electrocatalytic activity of the material is not yet explored to a substantial extent and rather hypothesized on the basis of experimental observation and physical reasoning.

Photocatalytic Applications. Application of carbon-based materials in photocatalysis has increasingly gained attention. Carbon-based materials have been frequently used as supports for the immobilization of active catalysts. Besides that, carbonaceous material enables fast mass transfer and can act as an active catalyst due to its electronic structure.[95,96] Moreover, N-doping of carbon materials assists in enhancing the photocatalytic activity of the materials by improving the conductivity, light absorption ability, and visible light sensitivity.[97] For example, a N-doped graphene/CdS nanocomposite depicted high photocatalytic efficiency for H_2 generation (210 μmol h^{-1}) compared to pure CdS (40 μmol h^{-1}).[98] This is attributed to the enhanced electrical conductivity of graphene due to N-doping that enables photoinduced charge transfer, avoiding the recombination of electron−hole pairs and increases photocatalytic activity.[99]

Furthermore, Mou and coworkers[100] reported that the photocatalytic efficiency of a N-doped graphene (NGR)/TiO_2 composite was greatly enhanced for H_2 production (13.3 μmol h^{-1}) as compared to pristine titania (7.1 μmol h^{-1}) and TiO_2/undoped graphene composites (8.9 μmol h^{-1}) under ultraviolet to near-infrared light. The improved photocatalytic efficiency of NGR/TiO_2 was due to to the formation of an interfacial contact between titania nanoparticles and graphene, as N-doping provides nucleation sites for titania nanoparticles on graphene sheets. Moreover, the electrical conductivity of NGR/TiO_2 has also increased after N-doping which was due to the recovery of a sp_2 graphite network ensuring effective charge transfer and charge separation.[100] The mechanism for photocatalytic hydrogen production on a NGR/TiO_2 composite is depicted in Figure 13. Triethanolamine (TEOA) played the role of a sacrificial agent in this reaction, whereas NGR not only acts as a scaffold for titania but also as a charge acceptor.[100]

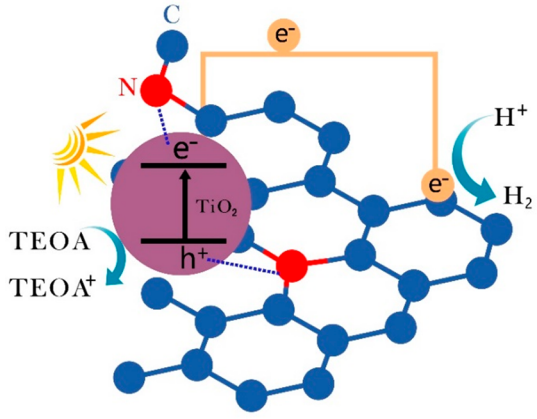

Figure 13. Schematic illustration for the strong coupling between TiO_2 and nitrogen atoms in NGR sheets and enhanced photoinduced charge transfer and photocatalytic hydrogen generation (TEOA stands for triethanolamine). Reprinted with permission from ref 100. Copyright (2014) American Chemical Society.

The photocatalytic activity of chitosan-derived graphene materials can also be improved via N-doping. The doping of nitrogen within the graphene structure modifies its electronic bands and may transform it into a semiconductor.[58] However, the magnitude of change in the electronic band structure depends on the amount of doped nitrogen. For 2−10 atom % of doped nitrogen, the band gap grows by 0.1−0.7 eV.[101] N-doping of graphene using chitosan aerogel beads via an in situ method (pyrolysis at 900 °C) imparts UV and visible light activity for hydrogen generation from methanol/water (30/70) mixtures.[57] Interestingly, the pyrolysis temperature plays a critical role in determining the photocatalytic activity of N-graphene (N(G)).

https://dx.doi.org/10.1021/acssuschemeng.9b07522
ACS Sustainable Chem. Eng. 2020, 8, 4708−4727

The increase in pyrolysis temperature (from 200 to 900 °C) helps in improving the crystallinity of N(G), thereby enhances the photocatalytic efficiency of N(G)-900 (entry 5, Table 2).

Table 2. Photocatalytic Activity of Chitosan-Derived N-Doped Graphene[a]

Entries	N(G)-T[a]	N content (wt %)	XPS graphenic C (%)	r^b (mmol g^{-1} h^{-1})	Evolved H_2 in 3 h (μmol)
1	N(G)-200	16.2	ND[b]	336	5.9
2	N(G)-400	15.8	ND	1497	15.9
3	N(G)-600	15.1	24.4	2633	16.7
4	N(G)-800	8.1	43.4	4999	55.2
5	N(G)-900	5.4	83.0	16,040	82.8

[a]N(G)-T[a] for hydrogen generation (initial reaction rate, r^b) from water/methanol mixtures under UV light (355 nm). N(G) pyrolysis temperature in °C.Reprinted with permission from ref 57. Copyright (2013) John Wiley and Sons. [b]ND: Not detected

However, it decreases the nitrogen content in N(G). This trend of activity could be rationalized on the basis of a decreased number of defects on the G-type structure with an increase in pyrolysis temperature. These defects are considered to be the determining factor for the photocatalytic efficiency of the (N)G materials for H_2 generation rather than the total nitrogen content. Table 2 summarizes the photocatalytic performance of N(G) for hydrogen evolution with respect to nitrogen content within N(G) and pyrolysis temperature used for preparation of samples.

In addition, the ability of N(G)-900 to absorb within the entire UV and visible range make it a visible light-active photocatalyst for hydrogen generation. However, it is difficult to calculate the band gap of N(G)-900 due to to its "neutral absorption", i.e., absorption within the entire UV−visible region. Surprisingly, the visible light (532 nm) activity of N(G) for hydrogen generation (~60 μmol after 3 h) is quite comparable with the activity shown in UV light (355 nm) under the same conditions. This comparable photocatalytic performance of N(G)-900 using different light sources is attributed to the similar light intensity used in both experiments (367 mW) and the neutral absorption spectrum of the photocatalyst.[57]

Furthermore, N-doped carbon as a support for metal nanoparticles (MNPs) improves the catalytic activity by increasing the number of chemically active sites on the catalyst due to carbon−metal binding. This can be rationalized considering that N-doped carbons assist in uniform dispersion of the MNPs and stabilize the MNPs by inhibiting agglomeration.[95] Besides that, C−N defects and N interstices at an adequate level may serve as local MNPs nucleation sites on a carbon support. Wu and coworkers[102] observed N-doped carbon-supported Ag/AgCl photocatalysts (Ag/AgCl/NC) effectively degrade Rhodamine B under visible light (420 nm) and attributed the activity to stable and uniform immobilization of Ag/AgCl nanoparticles over chitosan-derived N-doped carbon. Here, chitosan acts as both a reducing agent (to reduce silver ions to metallic silver nanoparticles) and stabilizing agent (to prevent agglomeration of nanoparticles).[102]

Organic semiconductors like g-C_3N_4 exhibit great potential in photocatalysis due to their striking optical properties like improved light harvesting capabilities.[103] However, the application of pristine g-C_3N_4 in photocatalysis is limited by its reduced charge mobility, fast rate of charge recombination, and insufficient electronic properties.[104] However, it has been discussed in this Perspective that N-doping improves the visible light absorption and electronic properties of the materials. In this context, chitosan has been discussed as a precursor for the synthesis of N-doped carbon materials or N-dopants. Interestingly, chitosan has also been explored as a C-dopant for the partial substitution of bridged N atoms in g-C_3N_4 with C atoms to improve visible light absorption and electron transport ability of g-C_3N_4. Surprisingly, C self-doping of g-C_3N_4 (introduction of C atom in g-C_3N_4 lattice during synthesis) using chitosan enhances the visible light (λ > 420 nm) absorption ability of the material which is attributed to the formation of delocalized π bonds among the adjacent heptazine rings which could promote charge separation and enhance the photocatalytic efficiency of g-C_3N_4. This may result in an increase in the photocatalytic efficiency of C self-doped g-C_3N_4 (CCCN) for H_2 evolution under visible light (entry 3, Table 3). CCCN showed a 7 times higher rate of H_2 generation (52.9 μmol h^{-1}) than pristine g-C_3N_4 (7.9 9 μmol h^{-1}). Platinum nanoparticles (Pt NPs) and triethanolamine (TEOA) were used as a cocatalyst and a sacrificial agent, respectively, in the hydrogen evolution experiment. The high efficiency of CCCN compared to pristine g-C_3N_4 is attributed to the electronic structure of CCCN (π bonds formation between the heptazine rings) acquired after the partial substitution of N with C atoms. In addition, doped carbon atoms may serve the role of a physical bridge as well as an electron bridge between adjacent heptazine rings (Figure 14). Consequently, charge transfer between the adjacent heptazine units occurred more swiftly in CCCN thereby increasing the photocatalytic efficiency of CCCN for H_2 evolution.[62]

Moreover, C self-doping through chitosan assists in controlling the morphology of g-C_3N_4 as well as the conduction band position by optimizing the carbon source content. Chitosan-derived honeycomb-like carbon-doped g-C_3N_4 denoted as CCN-0.2 (0.2 refers to the mass of chitosan in g) exhibited an enlarged specific surface area (130 m^2 g^{-1}) in comparison with pure g-C_3N_4 (9 m^2 g^{-1}). Additionally, CCN-0.2 showed a more negative conduction band position (2.5 eV) compared to pure g-C_3N_4 (2.7 eV) and better visible light absorption within the range of 450−700 nm. The honeycomb-like structure acquired after C-doping resulted in a higher specific surface area of CCN-0.2 offering more active sites and enhancing the interfacial charge transfer and charge separation efficiency.[50,105] These features are attributed to the increase in photocatalytic efficiency of CCN-0.2 (entry 4, Table 3) for hydrogen gas generation (using Pt NPs and TEOA as a cocatalyst and a sacrificial agent, respectively) compared to pristine g-C_3N_4. The rate of hydrogen gas generation observed for CCN-0.2 was 320 μmol h^{-1}, whereas the pristine g-C_3N_4 showed much lower activity with the rate of hydrogen gas generation 29 times less (11 μmol h^{-1}) than CCN-0.2.[50]

Inorganic semiconductors such as TiO_2 and ZnO are more commonly used in the field of heterogeneous photocatalysis than organic semiconductors like g-C_3N_4. The widespread use of these semiconductors is attributed to their nontoxicity, easy synthesis, insolubility, stability, remarkable optical properties, efficient photoactivity, and low cost.[106,107] Nevertheless, these metal oxides are active only under UV light ($\lambda \leq$ 390 nm) that restricts their application to utilize solar radiation. Additionally, they exhibit a fast rate of electron−hole recombination which further limits their application.[108]

The photochemical process involved in the degradation of organic dyes on ZnO and g-C_3N_4-chitosan beads and is illustrated in Figure 15a and b, respectively. The photo-

https://dx.doi.org/10.1021/acssuschemeng.9b07522
ACS Sustainable Chem. Eng. 2020, 8, 4708−4727

Table 3. Photocatalytic Application of Chitosan-Based N-Doped Carbon Materials

Entries	Photocatalyst	Synthesis method	Specific surface area (m^2g^{-1})	C−N bonding configurations	Light source	Photocatalytic Applications	ref
1	N-doped graphene	Pyrolysis	523	Pyridinic-N Pyridinium-N Pyridinic-N oxides	UV light (Nd:YAG laser 367 mW, λ = 355 nm)	Hydrogen generation (82.8 μmol)	57
2	Carbon quantum dots/graphitic carbon nitride nanosheets/cobalt complex	Hydrothermal method	NR[a]	Pyridinic-N Graphitic-N Aminic-N	Visible light (300 W xenon lamp, λ > 420 nm)	Hydrogen generation (295.9 μmol h^{-1} g^{-1})	63
3	Carbon-bridged g-C_3N_4	Supramolecular self-assembly method	24	Pyridinic-N Graphitic-N Aminic-N	Visible light (300 W xenon lamp, λ > 420 nm)	Hydrogen generation (52.9 μmol h^{-1})	62
4	Carbon-doped honeycomb-like graphitic carbon nitride	Supramolecular self-assembly method and calcination	130	Pyridinic-N Graphitic-N Aminic-N	Visible light (300 W xenon lamp, λ > 400 nm)	Hydrogen generation (320 μmol h^{-1})	50
5	Chitosan/TiO_2 composite	Solution cast method	03	NR	UV light (32W mercury lamp, λ = 365 nm)	Dye degradation 94%, for Reactive red 2 90% for Methylene blue 80% for Rhodamine B	114
6	Ag/AgCl/chitosan composites	One-step water bath heating method	NR	NR	Visible light (250 W xenon lamp, λ > 420 nm)	Dye degradation 96% for Rhodamine B	117
7	Chitosan-*g*- poly(acrylamide)/ZnS	Microwave-assisted method	NR	Aminic-N Amide-N	Simulated solar radiation	Dye degradation 75% for Congo red 69% for Methyl orange	118

[a]NR: Not reported.

https://dx.doi.org/10.1021/acssuschemeng.9b07522
ACS Sustainable Chem. Eng. 2020, 8, 4708−4727

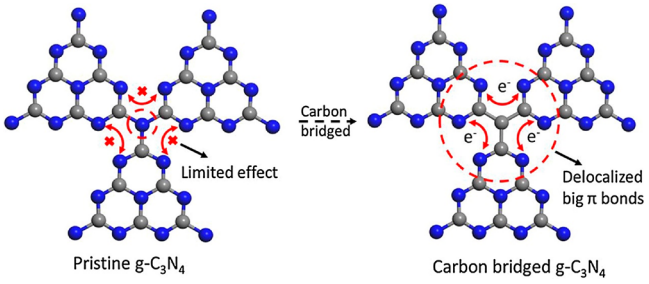

Figure 14. Scheme illustration of carbon-bridged g-C_3N_4 (C and N are indicated by gray and blue spheres, respectively). Reprinted with permission from ref 62. Copyright (2018) Elsevier.

degradation process was initiated by photoexcitation of the ZnO/g-C_3N_4-chitosan beads, followed by the generation of an electron−hole pair. The holes (h^+) may directly react with the dye molecules (Figure 15b) and oxidize them or may react with OH^- to produce hydroxyl radical species ($OH^•$). $OH^•$ species further react with the dye molecules; this results in either partial or complete degradation of the dyes (Figure 15a). Molecular O_2 reacts with an electron and forms a superoxide anion radical ($O_2^{-•}$). $O_2^{-•}$ species after protonation form a hydroperoxyl radical ($HO_2^•$). $HO_2^•$ species then subsequently react to form H_2O_2, which generates reactive hydroxyl radicals ($OH^•$) after dissociation. The hydroxyl radicals are very reactive and lead to degradation of the dye molecules.[109,110] The chitosan in the g-C_3N_4-chitosan beads may also act as an electron acceptor (Figure 15b); however, it is not proven with further data.[110]

Coupling these semiconductors with a carbon support and doping with nitrogen or carbon are possible ways to enhance the visible light absorption of TiO_2 and ZnO and reduce the rate of electron−hole recombination.[111] Moreover, the pore size of the support also plays a crucial role in controlling the growth of these metal oxide nanoparticles during synthesis and catalytic application thereby increasing the reactivity by allowing stabilization.[112] Chitosan-based composites of N- and S-doped TiO_2 (NST/CS) have shown high performance for photocatalytic degradation (91%) of tetracycline under visible light (after 20 min of illumination) compared to N- and S-doped TiO_2 (NST). The rate of photocatalytic degradation of tetracycline exhibited by NST/CS was 2 times higher than that of NST. The lower photocatalytic efficiency of NST compared to NST/CS is due to the direct binding of the tetracycline to the surface of NST that decreases the optical activity and consequently its photocatalytic efficiency, whereas chitosan, preventing a direct adsorption of tetracycline on the active sites, improves the photocatalytic performance of NST/CS.[113] A similar synergy between chitosan and TiO_2 has been observed by Farzana and Meenakshi[114] for the photocatalytic degradation of Reactive red 2 (RR), Methylene blue (MB), and Rhodamine B (RB) under UV light (365 nm) using a chitosan/TiO_2 composite (CTC). Here, the improved activity was attributed to chitosan, reducing the recombination of photogenerated charge carriers and also to its assistance in the adsorption of dye molecules increasing their availability to the active site (TiO_2) without blocking it.[114,115] CTC exhibited high photocatalytic activity with 94%, 90%, and 80% degradation efficiency for RR, MB, and RB, respectively, after 30 min of illumination,[108] whereas pure titania exhibited comparatively lower photocatalytic efficiency for the degradation of RR, MB, and RB (70%, 74%, and 45%, respectively).

The approach of preparing composite catalysts also provided a new insight for developing noble metal-free cocatalysts with significant photocatalytic activity for hydrogen production. For this, a visible light (450 nm)-active ternary photocatalyst has been prepared by chitosan-derived amino-functionalized carbon quantum dots (CQDs), graphitic carbon nitride nanosheets (CN), and cobalt complex (entry 2, Table 3). The photocatalyst was denoted as $Co(dcbpy)_2(NCS)_2$/CQDs/CN (dcbpy = (4,40-dicarboxy-2,20-bipyridine)). CQDs improve the mobility of photogenerated electrons. Simultaneously, the amido group of CQDs also established an amide bond with the carboxyl group of $Co(dcbpy)_2(NCS)_2$, while $Co(dcbpy)_2(NCS)_2$ accepts an electron from the conduction band of CN or CQDs. The distribution of the cobalt complexes over CN improved due to the amide bond formation thereby enhancing the hydrogen generation up to 295.9 μmol h^{-1} g^{-1} with an apparent quantum efficiency of 14.1%, whereas pristine CN was inactive under the same set of conditions.[63]

CONCLUSIONS AND FUTURE PERSPECTIVE

In conclusion, chitosan as a cheap, abundant, and renewable biomass resource rich in N content (~7 wt %) has vast potential for the preparation of N-doped carbon materials. This results from the functional groups of chitosan that offer a broad range of possibilities of chemical and mechanical modification. Numerous recent studies on the preparation and photocatalytic and

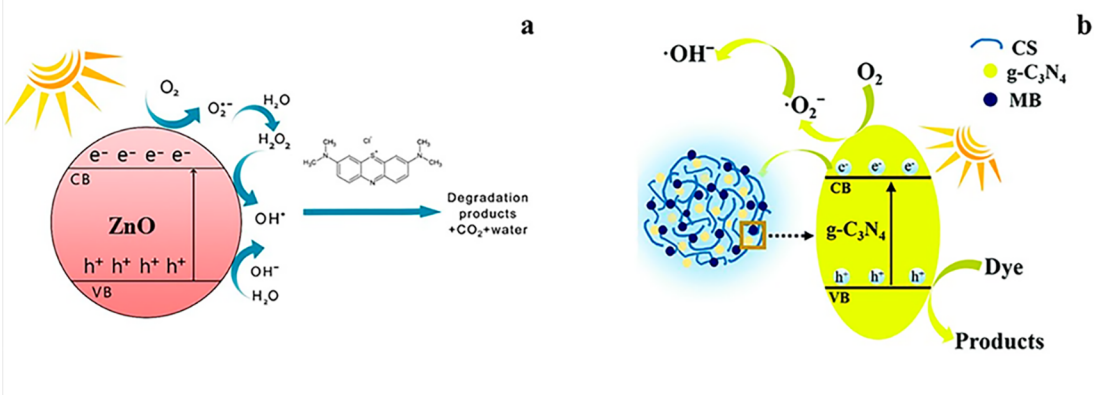

Figure 15. Photochemical processes involved in the degradation of organic dyes on (a) ZnO and (b) g-C_3N_4 (CS stands for chitosan beads and MB stands for Methylene blue). Panel (b) reprinted in part with permission from ref 110. Copyright (2018) Royal Society of Chemistry.

https://dx.doi.org/10.1021/acssuschemeng.9b07522
ACS Sustainable Chem. Eng. 2020, 8, 4708−4727

electrocatalytic applications of chitosan-derived N-doped carbon materials have been reviewed in this Perspective. Chitosan-based N-doped carbon materials can be prepared through a number of techniques such as CVD, hydrothermal carbonization, and postsynthesis treatment. Direct carbonization of chitosan results in the formation of graphene-like N-doped carbon materials. The process of carbonization has been assisted with chemical activation to prepare highly porous N-doped carbon materials. Direct carbonization incorporates nitrogen within the carbon structure, whereas chemical activation helps to increase the specific surface area of the N-doped carbon materials.

Some important features have been identified in chitosan-based N-doped carbon materials that are crucial for their electrocatalytic and photocatalytic activity. These features include (i) specific surface area and pore volume which are closely linked with the density of catalytically active sites and can to some extend be controlled via carbonization temperature, (ii) degree of graphitization that affects the activity of the catalyst by influencing the electron transfer resistance, (iii) C−N bonding configuration that has a unique potential for catalytic reactions attributed to different electronic structure and catalytically active sites, and (iv) contents of nitrogen and carbon and their electronic structures which are critical for charge separation efficiency and visible light absorption. Consequently, there is a need to develop scalable and economical synthesis methods to precisely control and acquire the ordered porous structures of chitosan-based N-doped carbon materials. More efforts are required to be made on controlling the C−N bonding configuration by adjusting N-doping and resulting defects for tunable electronic and chemical properties.

Nevertheless, promising results have been obtained with chitosan-based N-doped carbon materials for electrocatalytic reactions and specifically for the ORR in an alkaline medium. These are comparable or even superior to those of the noble metal-based commercial catalyst (Pt/C). However, there are limited studies that have explored the potential of chitosan-based N-doped carbon materials for the ORR in acidic media, which is attributed to their low activity and stability in acidic media compared to the commercial catalyst. Further studies are required to overcome these limitations. Moreover, chitosan-based N-doped carbon materials gained much attention for photocatalytic applications due to their visible light absorption. However, most of the reported studies use cocatalysts or require metal/metal oxide assistance (to prepare a composite) for improved photocatalytic hydrogen generation and contaminant degradation, respectively. These findings suggest the need for the development of new, more active, stable, and economically viable photocatalysts as an alternative to conventional UV light-active metal-based catalysts (TiO_2 and ZnO). Despite the visible light activity of chitosan-based N-doped carbon materials, there are few studies on their photocatalytic applications in the fields of hydrogen evolution and contaminant degradation. Moreover, this promising material class holds large potential for a wide range of photocatalytic applications such as biomass valorization, chemical synthesis, or CO_2 reduction.

AUTHOR INFORMATION

Corresponding Authors

Ayesha Khan − *Institute of Physical Chemistry, Polish Academy of Sciences, 01-224 Warsaw, Poland*; Email: akhan@ichf.edu.pl

Juan Carlos Colmenares − *Institute of Physical Chemistry, Polish Academy of Sciences, 01-224 Warsaw, Poland*; orcid.org/0000-0003-3701-6340; Email: jcarloscolmenares@ichf.edu.pl

Roger Gläser − *Institute of Chemical Technology, Leipzig University, 04103 Leipzig, Germany*; orcid.org/0000-0002-8134-4280; Email: roger.glaeser@uni-leipzig.de

Author

Michael Goepel − *Institute of Chemical Technology, Leipzig University, 04103 Leipzig, Germany*

Complete contact information is available at: https://pubs.acs.org/10.1021/acssuschemeng.9b07522

Notes

The authors declare no competing financial interest.

Biographies

Ayesha Khan received her M. Phil. in Environmental Sciences (2012) from PMAS Arid Agriculture University, Rawalpindi, Pakistan. After completion of her M. Phil., she worked as a teaching professional (2013-2017) at APSACS Fort Road, Rawalpindi, Pakistan. She is now pursuing her Ph.D. at the Institute of Physical Chemistry of the Polish Academy of Sciences, Warsaw, Poland. Her research interests primarily focus on the design of nanocomposites and their applications in the field of heterogeneous photocatalysis for biomass valorization.

Michael Goepel received his Ph.D. from the University of Leipzigin in 2014. He then moved to the Czech Republic for a postdoctoral stay. He returned to the University of Leipzig as postdoctoral researcher in 2016 to work in the group of Prof. Dr. Roger Gläser. His main research interests include heterogeneously catalyzed upgrading of biomass-based resources, photocatalysis, acid-redox-bifunctional catalysts, and investigations on mass-transfer-related phenomena in heterogeneous catalysis.

https://dx.doi.org/10.1021/acssuschemeng.9b07522
ACS Sustainable Chem. Eng. 2020, 8, 4708−4727

Juan Carlos Colmenares graduated from the Warsaw University of Technology (Chem. Eng., 1995) and obtained his M.Sc. (1997) in catalysis and Ph.D. (2004) in chemistry from the same university, and his habilitation (D.Sc., 2015) from the Institute of Physical Chemistry of the Polish Academy of Sciences. His interests range from materials science, nanotechnology, and catalysis to biomass/CO_2 valorization, solar chemicals, sonication, photocatalysis, and water/air purification. He worked as a postdoctoral fellow at the University of Córdoba, Spain (2005-2006, Prof. Marinas' group), and University of Southern California, United States (2006-2009, Nobel laureate Prof. G. A. Olah's group). He is a Marie Skłodowska-Curie fellow and member of the editorial advisory board for *Scientific Reports* and *Molecules* journals. Presently, he is working as an associate professor at the Institute of Physical Chemistry of the Polish Academy of Sciences in Poland.

Roger Gläser received his Ph.D. in chemistry from the University of Stuttgart. After a postdoctoral stay at the Georgia Institute of Technology, United States, he returned to the University of Stuttgart and completed his habilitation in Chemical Technology. Since 2007, he has been a full professor for chemical technology and the Director of the Institute of Chemical Technology at Leipzig University, Germany. His research interests include the preparation and characterization of novel catalysts with defined nanoporosity, after-treatment of diesel off-gas by SCR-based technologies, the utilization of renewable resources, photocatalysis, and diffusion in heterogeneous catalysis.

■ ACKNOWLEDGMENTS

This publication is part of a project that has received funding from the European Union's Horizon 2020 research and innovation programme under the Marie Skłodowska-Curie Grant Agreement No. 711859 and from the financial resources for science in the years 2017-2021 awarded for the implementation of an international cofinanced project. Roger Gläser and Michael Goepel gratefully acknowledge support from the Leipzig Graduate School of Natural Sciences, Building with Molecules and Nano-objects, as well as from the Research Academy Leipzig.

■ REFERENCES

(1) Varma, R. S. Biomass-derived renewable carbonaceous materials for sustainable chemical and environmental applications. *ACS Sustainable Chem. Eng.* **2019**, *7*, 6458−6470.
(2) Zahedifar, M.; Es-Haghi, A.; Zhiani, R.; Sadeghzadeh, S. M. Synthesis of benzimidazolones by immobilized gold nanoparticles on chitosan extracted from shrimp shells supported on fibrous phosphosilicate. *RSC Adv.* **2019**, *9*, 6494−6501.
(3) Jiang, Z.; Jiang, Z.-j.; Tian, X.; Chen, W. Amine-functionalized holey graphene as a highly active metal-free catalyst for the oxygen reduction reaction. *J. Mater. Chem. A* **2014**, *2*, 441−450.
(4) Gao, X.; Chen, X.; Zhang, J.; Guo, W.; Jin, F.; Yan, N. Transformation of chitin and waste shrimp shells into acetic acid and pyrrole. *ACS Sustainable Chem. Eng.* **2016**, *4*, 3912−3920.
(5) Yan, N.; Chen, X. Don't waste seafood waste. *Nature* **2015**, *524*, 155−157.
(6) Sivashankari, P. R.; Prabaharan, M. Deacetylation Modification Techniques of Chitin and Chitosan. In *Chitosan Based Biomaterials, Fundamentals*; Jennings, J. A., Bumgardner, J. D., Eds.; Elsevier: Cambridge, 2017; Vol. *1*, pp 117133. DOI: 10.1016/C2014-0-03147-4.
(7) Paulino, A. T.; Simionato, J. I.; Garcia, J. C.; Nozaki, J. Characterization of chitosan and chitin produced from silkworm crysalides. *Carbohydr. Polym.* **2006**, *64*, 98−103.
(8) Estevinho, B. N.; Rocha, F.; Santos, L.; Alves, A. Microencapsulation with chitosan by spray drying for industry applications -A review. *Trends Food Sci. Technol.* **2013**, *31*, 138−155.
(9) Jiang, T.; Deng, M.; James, R.; Nair, L. S.; Laurencin, C. T. Micro- and nanofabrication of chitosan structures for regenerative engineering. *Acta Biomater.* **2014**, *10*, 1632−1645.
(10) Bobbink, F. D.; Zhang, J.; Pierson, Y.; Chen, X.; Yan, N. Conversion of chitin derived N-acetyl-d-glucosamine (NAG) into polyols over transition metal catalysts and hydrogen in water. *Green Chem.* **2015**, *17*, 1024−1031.
(11) Kumar, R. M. N. A Review of Chitin and Chitosan Applications. *React. Funct. Polym.* **2000**, *46*, 1−27.
(12) Kumar, M. N.; Muzzarelli, R. A.; Muzzarelli, C.; Sashiwa, H.; Domb, A. J. Chitosan chemistry and pharmaceutical perspectives. *Chem. Rev.* **2004**, *104*, 6017−6084.
(13) Shukla, S. K.; Mishra, A. K.; Arotiba, O. A.; Mamba, B. B. Chitosan-based nanomaterials: A state-of-the-art review. *Int. J. Biol. Macromol.* **2013**, *59*, 46−58.
(14) Liu, Q.; Duan, Y.; Zhao, Q.; Pan, F.; Zhang, B.; Zhang, J. Direct synthesis of nitrogen-doped carbon nanosheets with high surface area and excellent oxygen reduction performance. *Langmuir* **2014**, *30*, 8238−8245.
(15) Zhang, Y.; Zhu, J. Y.; Ren, H. B.; Bi, Y. T.; Zhang, L. Facile synthesis of nitrogen-doped graphene aerogels functionalized with chitosan for supercapacitors with excellent electrochemical performance. *Chin. Chem. Lett.* **2017**, *28*, 935−942.
(16) Wu, T. X.; Wang, G. Z.; Zhang, X.; Chen, C.; Zhang, Y. X.; Zhao, H. J. Transforming chitosan into N-doped graphitic carbon electrocatalysts. *Chem. Commun.* **2015**, *51*, 1334−1337.
(17) Kumar, S.; Aziz, S. K. T.; Girshevitz, O.; Nessim, G. D. One-step synthesis of N-doped graphene quantum dots from chitosan as a sole precursor using chemical vapor deposition. *J. Phys. Chem. C* **2018**, *122*, 2343−2349.
(18) Guibal, E. Heterogeneous catalysis on chitosan-based materials: a review. *Prog. Polym. Sci.* **2005**, *30*, 71−109.
(19) Macquarrie, D. J.; Hardy, J. J. E. Applications of functionalized chitosan in catalysis. *Ind. Eng. Chem. Res.* **2005**, *44*, 8499−8520.
(20) Wang, D. W.; Su, D. Heterogeneous nanocarbon materials for oxygen reduction reaction. *Energy Environ. Sci.* **2014**, *7*, 576−591.

https://dx.doi.org/10.1021/acssuschemeng.9b07522
ACS Sustainable Chem. Eng. 2020, 8, 4708−4727

(21) Zhou, Y.; Zhang, L.; Huang, W.; Kong, Q.; Fan, X.; Wang, M.; Shi, J. N-doped graphitic carbon-incorporated g-C_3N_4 for remarkably enhanced photocatalytic H_2 evolution under visible light. *Carbon* **2016**, *99*, 111−117.
(22) Yeh, T. F.; Teng, C. Y.; Chen, S. J.; Teng, H. Nitrogen-doped graphene oxide quantum dots as photocatalysts for overall water-splitting under visible light illumination. *Adv. Mater.* **2014**, *26*, 3297−3303.
(23) Cong, S.; Zhao, Z. *Visible-Light Photocatalysis of Carbon-Based Materials Carbon Quantum Dots: A Component of Efficient Visible Light Photocatalysts*; IntechOpen: London, 2018. DOI: 10.5772/intechopen.70801.
(24) Inagaki, M.; Toyoda, M.; Soneda, Y.; Morishita, T. Nitrogen-doped carbon materials. *Carbon* **2018**, *132*, 104−140.
(25) Yadav, R.; Dixit, C. K. Synthesis, characterization and prospective applications of nitrogen-doped graphene: A short review. *J. Sci.: Adv. Mater. Devices* **2017**, *2*, 141−149.
(26) Granzier-Nakajima, T.; Fujisawa, K.; Anil, V.; Terrones, M.; Yeh, Y.-T. Controlling nitrogen doping in graphene with atomic precision: synthesis and characterization. *Nanomaterials* **2019**, *9*, 425−443.
(27) Ilnicka, A.; Lukaszewicz, J. P.; Shimanoe, K.; Yuasa, M. Urea treatment of nitrogen-doped carbon leads to enhanced performance for the oxygen reduction reaction. *J. Mater. Res.* **2018**, *33*, 1612−1624.
(28) Rybarczyk, M. K.; Lieder, M.; Jablonska, M. N-doped mesoporous carbon nanosheets obtained by pyrolysis of a chitosan−melamine mixture for the oxygen reduction reaction in alkaline media. *RSC Adv.* **2015**, *5*, 44969−44977.
(29) Zeng, L.; Qin, C.; Wang, L.; Li, W. Volatile compounds formed from the pyrolysis of chitosan. *Carbohydr. Polym.* **2011**, *83*, 1553−1557.
(30) Marsh, H.; Rodríguez, R. F. *Activated Carbon*, 1st ed., Elsevier: London, 2006.
(31) Verma, S.; Nadagouda, M. N.; Varma, R. S. Porous nitrogen-enriched carbonaceous material from marine waste: chitosan-derived carbon nitride catalyst for aerial oxidation of 5-hydroxymethylfurfural (HMF) to 2,5-furandicarboxylic acid. *Sci. Rep.* **2017**, *7*, 1−6.
(32) Primo, A.; Atienzar, P.; Sanchez, E.; Delgado, J. M.; García, H. From biomass wastes to large-area, high-quality, N-doped graphene: catalyst-free carbonization of chitosan coatings on arbitrary substrates. *Chem. Commun.* **2012**, *48*, 9254−9256.
(33) Fu, P.; Zhou, L.; Sun, L.; Huang, B.; Yuan, Y. Nitrogen-doped porous activated carbon derived from cocoon silk as a highly efficient metal-free electrocatalyst for the oxygen reduction reaction. *RSC Adv.* **2017**, *7*, 13383−13389.
(34) Singh, G.; Kim, I. Y.; Lakhi, K. S.; Joseph, S.; Srivastava, P.; Naidu, R.; Vinu, A. Heteroatom functionalized activated porous biocarbons and their excellent performance for CO_2 capture at high pressure. *J. Mater. Chem. A* **2017**, *5*, 21196−21204.
(35) Fan, X.; Zhang, L.; Zhang, G.; Shu, Z.; Shi, J. Chitosan derived nitrogen-doped microporous carbons for high performance CO_2 capture. *Carbon* **2013**, *61*, 423−430.
(36) Prasanna, K.; Subburaj, T.; Jo, Y. N.; Santhoshkumar, P.; Karthikeyan, S. K. S. S.; Vediappan, K.; Gnanamuthu, R. M.; Lee, C. W. Chitosan complements entrapment of silicon inside nitrogen doped carbon to improve and stabilize the capacity of Li-ion batteries. *Sci. Rep.* **2019**, *9*, 1−13.
(37) Fang, G.; Kaneko, S.; Liu, W.; Xia, B.; Sun, H.; Zhang, R.; Zheng, J.; Li, D. Facile synthesis of nitrogen-doped carbon coated $CoSnO_3$ via hydrothermal carbonization of carboxylated chitosan as anode materials for lithium-ion batteries. *Appl. Surf. Sci.* **2013**, *283*, 963−967.
(38) Yan, X. M.; Kang, J.; Gao, L.; Xiong, L.; Mei, P. Solvothermal synthesis of carbon coated N-doped TiO_2 nanostructures with enhanced visible light catalytic activity. *Appl. Surf. Sci.* **2013**, *265*, 778−783.
(39) Stout, R. L. Solvents in Today's Coatings. In *Applied Polymer Science: 21st Century*; Craver, C. D.; Carraher, C. E., Eds.; Elsevier: Kidlington, 2000; pp 527−543. DOI: 10.1016/B978-0-08-043417-9.X5000-4.
(40) Zhao, X.; Zhu, J.; Liang, L.; Li, C.; Liu, C.; Liao, J.; Xing, W. Biomass-derived N-doped carbon and its application in electrocatalysis. *Appl. Catal., B* **2014**, *154-155*, 177−182.
(41) Marroquin, J. B.; Rhee, K.Y.; Park, S.J. Chitosan nanocomposite films: Enhanced electrical conductivity, thermal stability, and mechanical properties. *Carbohydr. Polym.* **2013**, *92*, 1783−1791.
(42) Lee, J. H.; Marroquin, J.; Rhee, K. Y.; Park, S. J.; Hui, D. Cryomilling application of graphene to improve material properties of graphene/chitosan nanocomposites. *Composites, Part B* **2013**, *45*, 682−687.
(43) Lai, G. S.; Zhang, H. L.; Han, D. Y. Electrocatalytic oxidation and voltammetric determination of dopamine at a Nafion/carbon-coated iron nanoparticles-chitosan composite film modified electrode. *Microchim. Acta* **2008**, *160*, 233−239.
(44) Wang, Y.; Shao, Y.; Matson, D. W.; Li, J.; Lin, Y. Nitrogen-doped graphene and its application in electrochemical biosensing. *ACS Nano* **2010**, *4*, 1790−1798.
(45) Kumar, S.; Gonen, S.; Friedman, A.; Elbaz, L.; Nessim, G. D. Doping and reduction of graphene oxide using chitosan-derived volatile N-heterocyclic compounds for metal-free oxygen reduction reaction. *Carbon* **2017**, *120*, 419−426.
(46) Zeng, L.; Qin, C.; Wang, L.; Li, W. Volatile compounds formed from the pyrolysis of chitosan. *Carbohydr. Polym.* **2011**, *83*, 1553−1557.
(47) Inagaki, M.; Kang, F. Introduction. In *Materials Science and Engineering of Carbon: Characterization*; Inagaki, M., Kang, F., Eds.; Elsevier: Cambridge, 2016; p 3.
(48) Guo, D.; Wei, H.; Chen, X.; Liu, M.; Ding, F.; Yang, Z.; Yang, Y.; Wang, S.; Yang, K.; Huang, S. 3D hierarchical nitrogen-doped carbon nanoflower derived from chitosan for efficient electrocatalytic oxygen reduction and high performance lithium−sulfur batteries. *J. Mater. Chem. A* **2017**, *5*, 18193−18206.
(49) Zhang, Y.; Lu, L.; Zhang, S.; Lv, Z.; Yang, D.; Liu, J.; Chen, Y.; Tian, X.; Jin, H.; Song, W. Biomass chitosan derived cobalt/nitrogen doped carbon nanotubes for the electrocatalytic oxygen reduction reaction. *J. Mater. Chem. A* **2018**, *6*, 5740−5745.
(50) Liu, G.; Xue, M.; Liu, Q.; Yang, H.; Zhou, Y. Carbon doped honeycomb-like graphitic carbon nitride for photocatalytic hydrogen production. *J. Colloid Interface Sci.* **2019**, *552*, 728−734.
(51) Shao, Y.; Cao, C.; Chen, S.; He, M.; Fang, J.; Chen, J.; Li, X.; Li, D. Investigation of nitrogen doped and carbon species decorated TiO_2 with enhanced visible light photocatalytic activity by using chitosan. *Appl. Catal., B* **2015**, *179*, 344−351.
(52) Schmitt, M.; Fernandes, C. P.; da Cunha Neto, J. A.B.; Wolf, F. G.; dos Santos, V. S.S. Characterization of pore systems in seal rocks using nitrogen gas adsorption combined with mercury injection capillary pressure techniques. *Mar. Pet. Geol.* **2013**, *39*, 138−149.
(53) Wu, D.; Shi, Y.; Jing, H.; Wang, X.; Song, X.; Si, D.; Liang, S.; Hao, C. Tea-leaf-residual derived electrocatalyst: Hierarchical pore structure and self nitrogen and fluorine co-doping for efficient oxygen reduction reaction. *Int. J. Hydrogen Energy* **2018**, *43*, 19492−19499.
(54) He, Y.; Jiang, W. J.; Zhang, Y.; Huang, L. B.; Hu, J. S. Pore-structure-directed CO_2 electroreduction to formate on SnO_2/C catalysts. *J. Mater. Chem. A* **2019**, *7*, 18428−18433.
(55) Lee, S. H.; Kim, J.; Chung, D. Y.; Yoo, J. M.; Lee, H. S.; Kim, M. J.; Mun, B. S.; Kwon, S. G.; Sung, Y. E.; Hyeon, T. Design principle of Fe−N-C electrocatalysts: How to optimize multimodal porous structures? *J. Am. Chem. Soc.* **2019**, *141*, 2035−2045.
(56) Gao, M.; Zhu, L.; Ong, W. L.; Wang, J.; Ho, G. W. Structural design of TiO_2-based photocatalyst for H_2 production and degradation applications. *Catal. Sci. Technol.* **2015**, *5*, 4703−4726.
(57) Lavorato, C.; Primo, A.; Molinari, R.; Garcia, H. N-doped graphene derived from biomass as a visible-light photocatalyst for hydrogen generation from water/methanol mixtures. *Chem. - Eur. J.* **2014**, *20*, 187−194.
(58) Wei, D.; Liu, Y.; Wang, Y.; Zhang, H.; Huang, L.; Yu, G. Synthesis of N-doped graphene by chemical vapor deposition and its electrical properties. *Nano Lett.* **2009**, *9*, 1752−1758.

(59) Ferrari, A. C.; Robertson, J. Interpretation of Raman spectra of disordered and amorphous carbon. *Phys. Rev. B: Condens. Matter Mater. Phys.* **2000**, *61*, 14095−14107.
(60) Zhang, L.; Niu, J.; Dai, L.; Xia, Z. Effect of microstructure of nitrogen-doped graphene on oxygen reduction activity in fuel cells. *Langmuir* **2012**, *28*, 7542−7550.
(61) Xing, W.; Li, C.; Chen, G.; Han, Z.; Zhou, Y.; Hu, Y.; Meng, Q. Incorporating a novel metal-free interlayer into g-C_3N_4 framework for efficiency enhanced photocatalytic H_2 evolution activity. *Appl. Catal., B* **2017**, *203*, 65−71.
(62) Li, H.; Li, F.; Wang, Z.; Jiao, Y.; Liu, Y.; Wang, P.; Zhang, X.; Qin, X.; Dai, Y.; Huang, B. Fabrication of carbon bridged g-C_3N_4 through supramolecular self-assembly for enhanced photocatalytic hydrogen evolution. *Appl. Catal., B* **2018**, *229*, 114−120.
(63) Zhang, Y.; Zhang, W. D. Ternary catalysts based on amino-functionalized carbon quantum dots, graphitic carbon nitride nanosheets and cobalt complex for efficient H_2 evolution under visible light irradiation. *Carbon* **2019**, *145*, 488−500.
(64) Wu, Y. P.; Fang, S.; Jiang, Y.; Holze, R. Effects of doped sulfur on electrochemical performance of carbon anode. *J. Power Sources* **2002**, *108*, 245−249.
(65) Lam, E.; Luong, J. H. T. Carbon materials as catalyst supports and catalysts in the transformation of biomass to fuels and chemicals. *ACS Catal.* **2014**, *4*, 3393−3410.
(66) Serp, P.; Machado, B. *Nanostructured Carbon Materials for Catalysis*; RSC: Cambridge, 2015. DOI: 10.1039/9781782622567.
(67) Yan, Y.; Miao, J.; Yang, Z.; Xiao, F.-X.; Yang, H. B.; Liu, B.; Yang, Y. Carbon nanotube catalysts: recent advances in synthesis, characterization and applications. *Chem. Soc. Rev.* **2015**, *44*, 3295−3346.
(68) Suen, N. T.; Hung, S. F.; Quan, Q.; Zhang, N.; Xu, Y. J.; Chen, H. M. Electrocatalysis for oxygen evolution reaction: recent development and future perspectives. *Chem. Soc. Rev.* **2017**, *46*, 337−365.
(69) Graglia, M.; Pampel, J.; Hantke, T.; Fellinger, T. P.; Esposito, D. Nitro lignin-derived nitrogen-doped carbon as an efficient and sustainable electrocatalyst for oxygen reduction. *ACS Nano* **2016**, *10*, 4364−4371.
(70) Yuan, H.; Deng, L.; Cai, X.; Zhou, S.; Chen, Y.; Yuan, Y. Nitrogen-doped carbon sheets derived from chitin as non-metal bifunctional electrocatalysts for oxygen reduction and evolution. *RSC Adv.* **2015**, *5*, 56121−56129.
(71) Chhetri, B. P.; Soni, D.; RanguMagar, A. B.; Parnell, C. M.; Wayland, H.; Watanabe, F.; Kannarpady, G.; Biris, A. S.; Ghosh, A. Synthesis, characterization, and photocatalytic activity of N-doped carbonaceous material derived from cellulose in textile dye remediation. *J. Environ. Chem. Eng.* **2017**, *5*, 2586−2596.
(72) Kumar, A.; Kumar, A.; Sharma, G.; Naushad, M.; Stadler, F. J.; Ghfar, A. A.; Dhiman, P.; Saini, R. V. Sustainable nano-hybrids of magnetic biochar supported g-C_3N_4/$FeVO_4$ for solar powered degradation of noxious pollutants- Synergism of adsorption, photocatalysis and photo-ozonation. *J. Cleaner Prod.* **2017**, *165*, 431−451.
(73) Wang, D.; Liu, S.; Wang, J.; Lin, R.; Kawasaki, M.; Rus, E.; Silberstein, K. E.; Lowe, M. A.; Lin, F.; Nordlund, D.; Liu, H.; Muller, D. A.; Xin, H. L.; Abruña, H. D. Spontaneous incorporation of gold in palladium-based ternary nanoparticles makes durable electrocatalysts for oxygen reduction reaction. *Nat. Commun.* **2016**, *7*, 1−9.
(74) Daems, N.; Sheng, X.; Vankelecom, I. F. J.; Pescarmona, P. P. Metal-free doped carbon materials as electrocatalysts for the oxygen reduction reaction. *J. Mater. Chem. A* **2014**, *2*, 4085−4110.
(75) Niu, W.-J.; Zhu, R.-H.; Yan-Hua; Zeng, H.-B.; Cosnier, S.; Zhang, X.-J.; Shan, D. One-pot synthesis of nitrogen-rich carbon dots decorated graphene oxide as metal-free electrocatalyst for oxygen reduction reaction. *Carbon* **2016**, *109*, 402−410.
(76) Dai, L.; Xue, Y.; Qu, L.; Choi, H. J.; Baek, J. B. Metal-free catalysts for oxygen reduction reaction. *Chem. Rev.* **2015**, *115*, 4823−4892.
(77) Gong, K.; Du, F.; Xia, Z.; Durstock, M.; Dai, L. Nitrogen-doped carbon nanotube arrays with high electrocatalytic activity for oxygen. *Science* **2009**, *323*, 760−764.
(78) Guo, D.; Shibuya, R.; Akiba, C.; Saji, S.; Kondo, T.; Nakamura, J. Active sites of nitrogen-doped carbon materials for oxygen reduction reaction clarified using model catalysts. *Science* **2016**, *351*, 361−365.
(79) Qiao, M.; Meysami, S. S.; Ferrero, G. A.; Xie, F.; Meng, H.; Grobert, N.; Titirici, M. M. Low-cost chitosan-derived n-doped carbons boost electrocatalytic activity of multiwall carbon nanotubes. *Adv. Funct. Mater.* **2018**, *28*, 1707284−1707291.
(80) Qu, D. Investigation of oxygen reduction on activated carbon electrodes in alkaline solution. *Carbon* **2007**, *45*, 1296−1301.
(81) Li, J.-C.; Hou, P.-X.; Shi, C.; Zhao, S.-Y.; Tang, D.-M.; Cheng, M.; Liu, C.; Cheng, H.-M. Hierarchically porous Fe-N-doped carbon nanotubes as efficient electrocatalyst for oxygen reduction. *Carbon* **2016**, *109*, 632−639.
(82) Tao, G.; Zhang, L.; Chen, L.; Cui, X.; Hua, Z.; Wang, M.; Wang, J.; Chen, Y.; Shi, J. N-doped hierarchically macro/mesoporous carbon with excellent electrocatalytic activity and durability for oxygen reduction reaction. *Carbon* **2015**, *86*, 108−117.
(83) Xiao, M.; Zhu, J.; Feng, L.; Liu, C.; Xing, W. Meso/macroporous nitrogen-doped carbon architectures with iron carbide encapsulated in graphitic layers as an efficient and robust catalyst for the oxygen reduction reaction in both acidic and alkaline solutions. *Adv. Mater.* **2015**, *27*, 2521−2527.
(84) Hu, Y.; Jensen, J. O.; Zhang, W.; Cleemann, L. N.; Xing, W.; Bjerrum, N. J.; Li, Q. Hollow spheres of iron carbide nanoparticles encased in graphitic layers as oxygen reduction catalysts. *Angew. Chem.* **2014**, *126*, 3749−3753.
(85) Xie, S.; Huang, S.; Wei, W.; Yang, X.; Liu, Y.; Lu, X.; Tong, Y. Chitosan waste-derived Co and N co-doped carbon electrocatalyst for efficient oxygen reduction reaction. *ChemElectroChem* **2015**, *2*, 1806−1812.
(86) Lin, L.; Zhu, Q.; Xu, A. W. Noble-metal-free Fe-N/C catalyst for highly efficient oxygen reduction reaction under both alkaline and acidic conditions. *J. Am. Chem. Soc.* **2014**, *136*, 11027−11033.
(87) Lv, Q.; Si, W.; He, J.; Sun, L.; Zhang, C.; Wang, N.; Yang, Z.; Li, X.; Wang, X.; Deng, W.; Long, Y.; Huang, C.; Li, Y. Selectively nitrogen-doped carbon materials as superior metal-free catalysts for oxygen reduction. *Nat. Commun.* **2018**, *9*, 1−11.
(88) Liu, R.; Wu, D.; Feng, X.; Müllen, K. Nitrogen-doped ordered mesoporous graphitic arrays with high electrocatalytic activity for oxygen reduction. *Angew. Chem., Int. Ed.* **2010**, *49*, 2565−2569.
(89) Huang, W.; Wang, H.; Zhou, J.; Wang, J.; Duchesne, P. N.; Muir, D.; Zhang, P.; Han, N.; Zhao, F.; Zeng, M.; Zhong, J.; Jin, C.; Li, Y.; Lee, S.-T.; Dai, H. Highly active and durable methanol oxidation electrocatalyst based on the synergy of platinum−nickel hydroxide−graphene. *Nat. Commun.* **2015**, *6*, 1−8.
(90) Wu, G.; Swaidan, R.; Li, D.; Li, N. Enhanced methanol electro-oxidation activity of Pt Ru catalysts supported on heteroatom-doped carbon. *Electrochim. Acta* **2008**, *53*, 7622−7629.
(91) Wang, Y.; Li, Z.; Xu, S.; Lei, F.; Lin, S. One pot synthesis of Pt/Graphene composite using polyamidoamine/chitosan as a template and its electrocatalysis for methanol oxidation. *Catalysts* **2016**, *6*, 165.
(92) Guo, W.; Xu, L.; Li, F.; Xu, B.; Yang, Y.; Liu, S.; Sun, Z. Chitosan-assisted fabrication and electrocatalytic activity of the composite film electrode of heteropolytungstate/carbon nanotubes. *Electrochim. Acta* **2010**, *55*, 1523−1527.
(93) Zhou, Y.; Neyerlin, K.; Olson, T. S.; Pylypenko, S.; Bult, J.; Dinh, H. N.; Gennett, T.; Shao, Z.; O'Hayre, R. Enhancement of Pt and Pt-alloy fuel cell catalyst activity and durability via nitrogen-modified carbon supports. *Energy Environ. Sci.* **2010**, *3*, 1437−1446.
(94) Shao, Y.; Sui, J.; Yin, G.; Gao, Y. Gao, Y. Z. Nitrogen-doped carbon nanostructures and their composites as catalytic materials for proton exchange membrane fuel cell. *Appl. Catal., B* **2008**, *79*, 89−99.
(95) Li, X. H.; Antonietti, M. Metal nanoparticles at mesoporous N-doped carbons and carbon nitrides: functional Mott−Schottky heterojunctions for catalysis. *Chem. Soc. Rev.* **2013**, *42*, 6593−6604.
(96) Yang, M. Q.; Zhang, N.; Pagliaro, M.; Xu, Y. J. Artificial photosynthesis over graphene semiconductor composites. Are we getting better? *Chem. Soc. Rev.* **2014**, *43*, 8240−8254.

https://dx.doi.org/10.1021/acssuschemeng.9b07522
ACS Sustainable Chem. Eng. 2020, 8, 4708−4727

(97) Ge, J.; Zhang, Y.; Park, S. J. Recent advances in carbonaceous photocatalysts with enhanced photocatalytic performances: A mini review. *Materials* **2019**, *12*, 1916.
(98) Jia, L.; Wang, D. H.; Huang, Y. X.; Xu, A. W.; Yu, H. Q. Highly durable N-doped graphene/Cds nanocomposites with enhanced photocatalytic hydrogen evolution from water under visible light irradiation. *J. Phys. Chem. C* **2011**, *115*, 11466−11473.
(99) Zhang, N.; Yang, M. Q.; Liu, S.; Sun, Y.; Xu, Y. J. Waltzing with the versatile platform of graphene to synthesize composite photocatalysts. *Chem. Rev.* **2015**, *115*, 10307−10377.
(100) Mou, Z.; Wu, Y.; Sun, J.; Yang, P.; Du, Y.; Lu, C. TiO_2 nanoparticles-functionalized n-doped graphene with superior interfacial contact and enhanced charge separation for photocatalytic hydrogen generation. *ACS Appl. Mater. Interfaces* **2014**, *6*, 13798−13806.
(101) Rani, P.; Jindal, V. K. Designing band gap of graphene by B and N dopant atoms. *RSC Adv.* **2013**, *3*, 802−812.
(102) Wu, Y.; Chen, S.; Guo, X.; Wu, J.; Peng, B.; Liu, Z. Environmentally benign chitosan as precursor and reductant for synthesis of Ag/AgCl/N-doped carbon composite photocatalysts and their photocatalytic degradation performance. *Res. Chem. Intermed.* **2017**, *43*, 3677−3690.
(103) Zheng, Y.; Lin, L.; Ye, X.; Guo, F.; Wang, X. Helical graphitic carbon nitrides with photocatalytic and optical activities. *Angew. Chem., Int. Ed.* **2014**, *53*, 11926−11930.
(104) Shao, L.; Jiang, D.; Xiao, P.; Zhu, L.; Meng, S.; Chen, M. Enhancement of g-C_3N_4 nanosheets photocatalysis by synergistic interaction of ZnS microsphere and RGO inducing multistep charge transfer. *Appl. Catal., B* **2016**, *198*, 200−210.
(105) Huang, J.; Cheng, W.; Shi, Y.; Zeng, G.; Yu, H.; Gu, Y.; Shi, L.; Yi, K. Honeycomb-like carbon nitride through supramolecular preorganization of monomers for high photocatalytic performance under visible light irradiation. *Chemosphere* **2018**, *211*, 324−334.
(106) Zainal, Z.; Hui, L. K.; Hussein, M. Z.; Abdullah, A. H.; Hamadneh, I. M. Characterization of TiO_2−chitosan/ glass photocatalyst for the removal of a monoazo dye via photodegradation−adsorption process. *J. Hazard. Mater.* **2009**, *164*, 138−145.
(107) Riente, P.; Noël, T. Application of metal oxide semiconductors in light-driven organic transformations. *Catal. Sci. Technol.* **2019**, *9*, 5186−5232.
(108) Zhu, H.; Jiang, R.; Fu, Y.; Guan, Y.; Yao, J.; Xiao, L.; Zeng, G. Effective photocatalytic decolorization of methyl orange utilizing TiO_2/ZnO/chitosan nanocomposite films under simulated solar irradiation. *Desalination* **2012**, *286*, 41−48.
(109) Hairom, N. H. H.; Mohammad, A. W.; Ng, L. Y.; Kadhum, A. A. H. Utilization of self-synthesized ZnO nanoparticles in MPR for industrial dye wastewater treatment using NF and UF membrane. *Desalin. Water Treat.* **2015**, *54*, 944−955.
(110) Zhao, C.; Yan, Q.; Wang, S.; Dong, P.; Zhang, L. Regenerable g-C_3N_4−chitosan beads with enhanced photocatalytic activity and stability. *RSC Adv.* **2018**, *8*, 27516−27524.
(111) Dong, S.; Feng, J.; Fan, M.; Pi, Y.; Hu, L.; Han, X.; Liu, M.; Sun, J.; Sun, J. Recent developments in heterogeneous photocatalytic water treatment using visible light-responsive photocatalysts: a review. *RSC Adv.* **2015**, *5*, 14610−14630.
(112) Elbanna, O.; Fujitsuka, M.; Majima, T. g-C_3N_4/TiO_2 Mesocrystals composite for h2 evolution under visible-light irradiation and its charge carrier dynamics. *ACS Appl. Mater. Interfaces* **2017**, *9*, 34844−34854.
(113) Farhadian, N.; Akbarzadeh, R.; Pirsaheb, M.; Jen, T.-C.; Fakhri, Y.; Asadi, A. Chitosan modified N, S-doped TiO_2 and N, S-doped ZnO for visible light photocatalytic degradation of tetracycline. *Int. J. Biol. Macromol.* **2019**, *132*, 360−373.
(114) Farzana, M. H.; Meenakshi, S. Synergistic effect of chitosan and titanium dioxide on the removal of toxic dyes by the photodegradation technique. *Ind. Eng. Chem. Res.* **2014**, *53*, 55−63.
(115) Chen, A.; Zeng, G.; Chen, G.; Hu, X.; Yan, M.; Guan, S.; Shang, C.; Lu, L.; Zou, Z.; Xie, G. Novel thiourea-modified magnetic ion imprinted chitosan/TiO_2 composite for simultaneous removal of cadmium and 2,4-dichlorophenol. *Chem. Eng. J.* **2012**, *191*, 85−94.
(116) El-Nagar, G. A.; Hassan, M. A.; Fetyan, A.; Kayarkatte, M. K.; Lauermann, I.; Roth, C. A promising N-doped carbon-metal oxide hybrid electrocatalyst derived from crustacean's shells: Oxygen reduction and oxygen evolution. *Appl. Catal., B* **2017**, *214*, 137−147.
(117) Wang, H.; Wu, Y.; Wu, P.; Chen, S.; Guo, X.; Meng, G.; Peng, B.; Wu, J.; Liu, Z. Environmentally benign chitosan as reductant and supporter for synthesis of Ag/AgCl/chitosan composites by one-step and their photocatalytic degradation performance under visible-light irradiation. *Front. Mater. Sci.* **2017**, *11*, 130−138.
(118) Pathania, D.; Gupta, D.; Al-Muhtaseb, A. H.; Sharma, G.; Kumar, A.; Naushad, M.; Ahamad, T.; Alshehri, S. M. Photocatalytic degradation of highly toxic dyes using chitosan-g-poly(acrylamide)/ZnS in presence of solar irradiation. *J. Photochem. Photobiol., A* **2016**, *329*, 61−68.

https://dx.doi.org/10.1021/acssuschemeng.9b07522
ACS Sustainable Chem. Eng. 2020, 8, 4708−4727